Mask Projection Microstereolithography 3D Printing of Gelatin Methacrylate

Wyatt Redmond Surbey

Thesis submitted to the faculty of the Virginia Polytechnic Institute and State University
in partial fulfillment of the requirements for the degree of

Master of Science
In
Materials Science and Engineering

Abby R Whittington
Johan E Foster
Hang Yu

April 9th, 2019
Blacksburg, VA

Keywords: 3D printing, GelMA, tissue engineering

Mask Projection Microstereolithography 3D Printing of Gelatin Methacrylate

Wyatt Surbey

ABSTRACT

Gelatin methacrylate (GelMA) is a ubiquitous biocompatible photopolymer used in tissue engineering and regenerative medicine due to its cost-effective synthesis, tunable mechanical properties, and cellular response. Biotechnology applications utilizing GelMA have ranged from developing cell-laden hydrogel networks to cell encapsulation and additive manufacturing (3D printing). However, extrusion based 3D printing is the most common technique used with GelMA. Mask projection microstereolithography (MPμSL or μSL) is an advanced 3D printing technique that can produce geometries with high resolution, high complexity, and feature sizes unlike extrusion based printing. There are few biomaterials available for μSL applications, so 3D printing GelMA using μSL would not only add to the repertoire materials, but also demonstrate the advantages of μSL over other 3D printing techniques. A novel GelMA resin was tested with μSL to create a porous scaffold with a height and print time that has not been displayed in the literature before for a scaffold of this size. The resin consists of GelMA, deionized water, lithium phenyl-2,4,6-trimethylbenzoylphosphinate (LAP, photoinitiator), and 2-Hydroxy-4-methoxybenzophenone-5-sulfonic acid (sulisobenzone, UV blocker) and can be processed at room temperature. Four resins were tested (w/w %) and characterized for μSL printing: 20% GelMA 0.5% UV blocker, 20% GelMA 1.0% UV blocker, 30% GelMA 0.5% UV Blocker, and 30% GelMA 1.0% UV blocker. Swell testing, working curve, photo-rheology, photo-DSC (dynamic scanning calorimetry), 3D printing, and cell culture tests were performed and results showed that 30% GelMA 1.0% UV blocker had the best 3D print fidelity among resin compositions.

Mask Projection Microstereolithography 3D Printing of Gelatin Methacrylate

Wyatt Surbey

GENERAL AUDIENCE ABSTRACT

Three dimensional (3D) printing is a widely used technology to rapidly produce structures with varying degrees of complexity. 3D printing of biological components is of interest because as the world population increases, there is a lack of donors available to compensate for organ loss and tissue replacement. 3D printing offers a solution to great custom scaffolds and structures that mimic physiological geometry and properties. One printing technique is known as microstereolithography, or μSL, which uses a projector-like system to pattern ultraviolet (UV) light in specific arrangements to generate complex geometries and 3D parts. Gelatin is a material of interest for this technology because gelatin is derived from collagen, which is the most abundant protein found in the body. Gelatin can be modified so that it is reactive with UV light, and can be processed with μSL to generate 3D structures. In this work, gelatin was modified into the form of gelatin methacrylate (GelMA) in order to develop and test resin formulations for use with μSL. Four different resins were tested and characterized and the results indicated that one GelMA resin produced prints with greater fidelity and resolution than other formulations. This resin has been identified for potential applications in tissue engineering and 3D printed organ development.

Dedication

I dedicate this thesis to my parents, Lisa and Glen Surbey who taught me everything I have needed to know in life thus far, and who have shown me the beauty of unconditional love. Through them I have blossomed into a young man ready to tackle the future and life at length. I will never forget the three most important things they taught me about life: God, family, and everything else.

Acknowledgements

I would first like to acknowledge my advisor, Dr. Abby Whittington for taking me on as a graduate student and seeing me through this process of growth and development. Additionally for tolerating my constant perfectionism as well as procrastination.

I would also like to acknowledge my committee members Dr. Johan Foster and Dr. Hang Yu for working with me throughout this project. Their feedback has been indispensable and encouraged me multiple times throughout this process.

Lastly I would like to thank the following people and laboratories for their assistance throughout this project: Nick Chartrain for his endless help and direction and significant contribution to the aims of this work, Casey Clark for his aid in GelMA synthesis and direction with this work, Dr. Christopher Williams and the DREAMS lab at Virginia Tech for the utilization of their space in Goodwin Hall, and Dr. Timothy Long for the use of his instrumentation and laboratory space in ICTAS II at Virginia Tech.

Table of Contents

List of Figures

Figure 3-15: Representative light microscopy images of GelMA films seeded with 3T3s and stained for nuclei (DAPI, blue) and actin (Texas Red, red). Experiments were run in triplicate (n = 3)

List of Tables

List of Abbreviations

Additive manufacturing (AM)

Rapid prototyping (RP)

Computer aided design (CAD)

Stereolithography (SL)

Mask projection microstereolithography (μSL)

Three dimensional (3D)

Two dimensional (2D)

Ultraviolet (UV)

Gelatin methacrylate (GelMA)

Extracellular matrix (ECM)

[3-(4,5-dimethylthiazol-2-yl)-5-(3-carboxymethoxyphenyl)-2-(4-sulfophenyl)-2H-tetrazolium (MTS)

Poly (propylene) fumarate (PPF)

Diethyl fumarate (DEF)

N-Vinylpyrrolidone (NVP)

Trimethylene carbonate (TMC)

Trimethylolpropane (TMP)

Polycaprolactone (PCL)

Polylactide (PLA)

Poly(ethylene glycol) diacrylate (PEG, PEGDA)

Poly d, l-lactic-glycolic acid (PLGA)

Poly(ethylene glycol) dimethacrylate (PEGDMA)

Oxidized methacrylic alginate (OMA)

Arginine, Glycine, and Aspartate (Arg-Gly-Asp, or RGD)

Poly(ethylene glycol) methyl ether methacrylate (PEGMEM)

Hyaluronic acid (HA)

Glycosaminoglycan (GAG)

Matrix metalloproteinases (MMPs)

Degree of functionalization (DF)

Degree of substitution (DS)

Degree of methacrylation (DM)

Phosphate buffered saline (PBS)

2-hydroxy-l-[4-(hydroxyethoxy)phenyl]-2-methyl-l-propanone (Irgacure 2959)

2,2-dimethoxy-2-phenylacetophenone (DMPA)

Lithium phenyl-2,4,6-trimethylbenzoylphosphinate (LAP)

2,2'-Azobis[2-methyl-N-(2-hydroxyethyl) propionamide] (VA-086)

Eosin Y/Triethanolamine/l-vinyl-2-pyrrolidinone (EY)

Methacrylated hyaluronic acid (HAMA)

Cellulose nanocrystals (CNCs)

Nuclear magnetic resonance (NMR) spectroscopy

Methacrylic anhydride (MA)

2-Hydroxy-4-methoxybenzophenone-5-sulfonic acid (sulisobenzone)

Deuterium oxide (D_2O)

Fetal bovine serum (FBS)

Deionized (DI) water

Photo-Differential Scanning Calorimetry (DSC)

Chapter 1: Introduction

1.1 An Introduction to 3D Printing

Additive manufacturing (AM), also known as three-dimensional (3D) printing has become a widely used technology across many fields of science and engineering. Originally deemed rapid prototyping (RP) because of its industrial applications for rapidly developing a prototype in which a final product can be built or commercialized upon – the term has since evolved to AM and 3D printing in the research field to describe technologies that create physical prototypes directly from digital model data [1]. In fact, many parts for industrial and research applications are directly manufactured using AM machines, thus labelling them as prototypes is inadequate [1]. The basic principle of AM technology is to take a 3D computer-aided-design (CAD) model and fabricate the part by adding consecutive layers [1]. This layer-by-layer approach is the anchor between AM techniques. How AM techniques differ lie in the type of materials that can be used, how the layers are generated, and how the layers are bonded to one another [1]. These differences determine factors like the accuracy of the final product, and both its material and mechanical properties [1]. Different AM techniques will also determine factors like how quickly the part can be made, how much post-processing of the part is required, the size of the AM machine used, and the overall cost of the AM machine and process [1]. For the purposes of this research, not all AM techniques will be described at length. However, it is important to realize that AM technologies have a wide range of applications and features with varying pros and cons. In this thesis, the focus will be on polymeric biomaterial resin development for the AM technique mask projection microstereolithography (also known as vat photopolymerization,

MPμSL, or μSL). As an introduction, first, a few competing AM technologies will be discussed: extrusion, inkjet, and laser-assisted 3D printing. Then, the significance and limitations of biomaterial development in AM will be discussed regarding extrusion, inkjet, and laser-assisted 3D printing. Lastly, μSL will be discussed at length with regards to a specific polymeric biomaterial (gelatin methacrylate, GelMA) and the aims to be addressed in this work.

1.2 AM Techniques

In AM, there are many alternative methods to extrusion 3D printing that each have their own unique advantages and disadvantages. These printing techniques differ in the materials that can be used, how the layers are created, and how the layers are bonded to each other. Such differences will determine factors like the accuracy of the final part plus its material properties and mechanical properties. They will also determine factors like how quickly the part can be made, how much post-processing is required, the size of the AM machine used, and the overall cost of the machine and process [2, 3]. Figure 1-1, presents a simplified schematic of AM printing technologies and their advantages/disadvantages in respect to considerations such as viscosity, resolution, and print speed. A bio-ink is different from a biomaterial in that bio-inks contain cells within their solution while biomaterials are stand-alone, but may incorporate cells after a scaffold is produced [2, 4-7]. For the purposes of this research, only biomaterial configurations will be considered, not bio-inks.

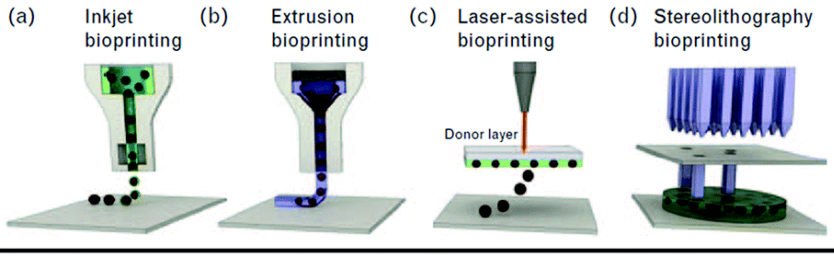

(e) Comparison of 3D bioprinting modalities

	Inkjet	Extrusion	Laser assisted	Stereolithography
Ink viscosity	3.5–12 mPa/s	Up to 6 x 10^7 mPa/s	1–300 mPa/s	No limitation
Cell density	Low, <10^6 cells/ml	No limitation	Medium, <10^8 cells/ml	No limitation
Resolution	High	Moderate	High	High
Print speed	Fast	Slow	Medium	Fast
Cost	Low	Medium	High	Low

Figure 1-1. Comparison of AM techniques that are used in bio-AM. Figure reproduced with publisher's permission [2].

Extrusion-based printing is the most widely used and well known technique; it uses a pneumatic or mechanical system in order to expel the material and create 2D patterns on a substrate [2]. These 2D patterns produced are then solidified either physically or chemically, and then the process is repeated to yield a 3D object or scaffold [2, 8]. When considering using extrusion-based printing for biomaterial production, the printability may depend on a variety of factors such as: the viscosity of the polymer, the temperature of the pneumatic or mechanical system used to expel the solution, or a potential crosslinking mechanism to solidify the layers post processing. Extrusion-based printing is also limited by the extrusion nozzle length and size. In general, the advantage of extrusion-based printing includes wide bio-ink/biomaterial selectivity (materials of varying viscosity and mechanical properties) [2]. However, a disadvantage of extrusion-based printing is that the overall resolution (feature sizes such as pores and layer thickness) is greater than 100 μm. Additionally, in order to reach higher resolution higher pressures and slower print speeds are required which slow down the overall process (on the

magnitude of hours depending on the part size). Figure 1-1 also depicts inkjet and laser assisted 3D printing. Inkjet printing existed first as a two-dimensional process via printing documents and images from computers, but evolved as a 3D printing method in which particles of material were deposited onto a substrate [1]. The process has since extended into acrylate photopolymers, in which droplets of liquid monomer are deposited and then exposed to ultraviolet (UV) light to photopolymerize [1]. As Figure 1-1 shows, the advantages of inkjet printing include low cost and high speed printing. Additionally inkjet printing allows for ease of multi-material printing, but the choice of materials is limited and the resolution and part accuracy is also limited as the scale of parts increases [1]. Inkjet printing can produce resolutions lower than 100 μm, but that resolution is sacrificed when printing constructs that are cm in size [1]. Additionally this process is much faster than extrusion printing, with constructs typically being printed in less than an hour [1]. Laser-assisted printing is similar to inkjet printing, but instead a donor layer is present from which the material is deposited. This donor layer allows for higher viscosity materials to be used, but the laser inherently increases the cost of the apparatus. Like inkjet printing, the primary limitation of laser-assisted printing is the lack of materials available. Laser-assisted printing also typically produces constructs in less than an hour and can reach resolutions lower than 100 μm [1].

The technique that particularly stands out in Figure 1-1 is stereolithography, because it comparatively has fewer limitations while providing higher resolution and faster print speeds at a lower cost. Stereolithography (SL), is a photochemical process in which light causes chemical monomers to link together to form polymers [2]. These polymers then make up the body of a three-dimensional solid. A more advanced technique of stereolithography is known as mask

projection microstereolithography, which will be referred as µSL for the remainder of this document. The µSL process is different than traditional SL in that instead of having a light source to scans across the vat of material and selectively curing points, there is a dynamic mask that patterns the light to expose an entire cross-section of the desired print at once [9]. Figure 1-2 provides an in-depth schematic of a µSL machine.

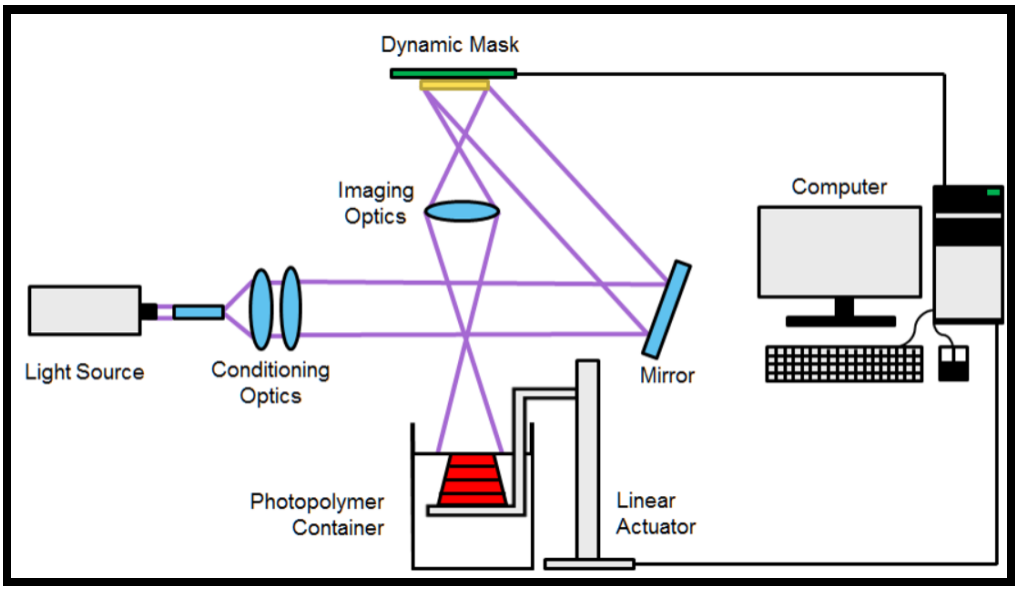

Figure 1-2. µSL system diagram, as described, a (typically UV) light source emits light at a specific wavelength which is then reflected and pattern via a mirror and dynamic mask onto the surface of a photopolymer container with a build stage containing cross-linkable resin. Figure reproduced with publisher's permission [9].

By exposing an entire cross-section at once, the printing time can be dramatically reduced [9]. In addition, the feature sizes of the print are not limited to the radius of the light source, meaning feature sizes smaller than 10 µm can be produced [9]. This small feature size is a huge advantage for µSL systems because scaffold shape and resolution directly affects cell-material interactions [6]. One of the primary limitations for µSL is material availability. Since most material development is targeted toward extrusion based printing, other 3D printing technologies tend to lack commercially available materials. This leaves space where there is a necessity for biomaterial development and 3D printability testing. This is just one reason this work will focus

on biomaterial development for stereolithography, more specifically: improving on gelatin methacrylate (GelMA) 3D printing in μSL. In order to do so, understanding biomaterial development in AM must be addressed.

1.3 Biomaterial Development in AM

In the biomedical engineering field, 3D printing is especially of interest for tissue engineering and regenerative medicine applications. Regenerative medicine encompasses tissue engineering, but both terms refer to the ability to create a functional tissue from either scaffolds, cells, and/or biologically active molecules in pursuit of curing damaged tissues or organs [7, 10]. In order to produce scaffolds, it is necessary to develop materials or biomaterials that are not only compatible with the human body, but also compatible with the variety of 3D printing systems available. The difference between a material and a biomaterial lies in the name itself: a biomaterial is a material (natural or synthetic) that is used in medical applications to support, enhance, or replace damaged tissue or a biological function [11]. Since AM techniques originated from engineering, they present challenges to materials scientists and chemists alike when developing new materials for use in AM [5]. Researchers are still understanding what makes a material "printable" and what they can do to optimize a material's printability [4, 5]. For example, in extrusion there might be considerations like the temperature of the pneumatic print head, or the print bed, but for μSL there might be considerations like laser intensity and build volume. Some researchers utilize rheological or mechanical characterization to narrow material selection by exploring material chemistry, such as ionic interactions and coordination bonds [5].

However, in general, printing and material considerations for AM specific to biomaterials can be broken down into three categories:

1. Shape and resolution (layer thickness – feature sizes)
2. Material heterogeneity (viscoelasticity, mechanical strength/integrity, curing mechanism, biocompatibility, print speed)
3. Cell-material interactions (degradation, cell fusion, structural changes) [6].

1.3.1 Shape and Resolution

Since µSL has such high control over tissue scaffold geometry and resolution, it could become a key player in continuing to understand mechanisms of the cellular environment and regenerative process [11]. µSL can obtain resolutions below 100 µm [3, 9]. Ideally, this would give researchers and engineers the ability to create a tissue engineering scaffold that not only mimics the structural properties of the extra cellular matrix (ECM), but also the *in vivo* transport mechanisms of water, oxygen, nutrients, and waste. However, the main impedance with µSL's capabilities is the repertoire of materials for use with µSL is limited in comparison to other AM techniques like extrusion [3, 4, 11, 12]. This lack of materials available also transcends to the characterization methods reported with µSL. Often in the literature, a scaffold or 3D printed part is imaged via optical photography or microscopy and reported utilizing a novel material system. However, the fidelity of prints are rarely seen analyzed or quantified via some type of fidelity metric. One method identified is to compare the .STL or CAD file to the produced part in order to assess the deviation from the CAD file [9]. Many researchers avoid critical analysis of their scaffolds, so there is a gap in the literature where the fidelity and repeatability of micro patterns, scaffolds, and other 3D generated parts is quantified.

1.3.2 Material Heterogeneity

Commercial (encompassing large scale and micro applications) stereolithography (SL) materials typically range from epoxies to acrylics, neither of which tend to be biocompatible or biodegradable [11, 13]. Since biocompatibility (meaning the surface of the scaffold will be chemically compatible with cells without inducing an immune response) and biodegradability (meaning the scaffold would degrade *in vivo* without causing an immune response) are key characteristics of tissue engineering scaffolds used in bio-AM, an alternative selection of SL materials have been researched (some of which are commercially available and some which are not) for µSL applications [4, 14]. Typically, these materials range from synthetic polymers to naturally derived polymers that have been modified to have photo-active groups such as acrylates and methacrylates, or a combination of the two [4].

1.3.3 Material Heterogeneity: Synthetic Polymers

One of the first notable synthetic polymers that was deemed biocompatible and biodegradable for use in µSL is poly(propylene fumarate) (PPF) which is typically crosslinked along with diethyl fumarate (DEF), methyl methacrylate, and N-vinylpyrrolidone (NVP) [3, 11, 14, 15]. DEF and NVP are added as diluents and lower the viscosity of the resulting resin, making the solution easier to process via µSL [11, 14]. However, these diluents can add toxicity into the environment and reduce biocompatibility [11]. Although PPF/DEF systems are attractive in bone tissue engineering they are limited in soft tissue applications due to their mechanical properties are similar to trabecular bone [15]. While numerous articles report osteogenic (bone tissue forming) regenerative effects using PPF/DEF, PPF/DEF soft tissue (nerves, muscles, blood vessels) applications are nearly non-existent [15, 16]. Thus, PPF/DEF is not a universal material

system for μSL. Lee *et al* demonstrated another novel photopolymer from trimethylene carbonate (TMC) trimethylolpropane (TMP) that demonstrated similar biocompatible and biodegradable properties to PPF, but with mechanical properties closer to cartilage [15, 17]. However, the resin still consists of diluents that cause toxicity upon degradation, and the mechanical properties are dependent on diluent concentrations [15]. Other notable synthetic biomaterial resins consist of: polycaprolactone (PCL), polylactide (PLA), acrylated or methacrylated poly(ethylene glycol) (PEG, PEG-DA, PEG-DMA), and poly d, l-lactic-glycolic acid (PLGA) [4, 11, 15, 18-21]. PCL has high elasticity and thermal properties, but limited cellular attachment due to its hydrophobicity [15, 19, 22]. PLA has shown biodegradability and μSL process-ability, but poor mechanical and thermal stability [19]. PEG (and its subsequently mentioned derivatives) is a relatively rigid photopolymer that exhibits excellent rheological properties for use in μSL; however, PEG is considered a bio-inert polymer meaning while it does not elicit an immune response, cells do not adhere to PEG scaffolds readily [2, 11, 21]. Lastly, PLGA holds similar properties to PCL and PLA but exhibits faster degradation and the degradation products can be toxic in high concentrations [22, 23]. Although synthetic polymers provide a wide avenue of material selection for materials scientists and chemists to manipulate and explore, their tailor-ability must match their biocompatible and biodegradable properties in order for them to be suitable in μSL tissue engineering applications. And, while most of the synthetic polymers mentioned do have μSL tissue engineering applications, synthetic polymers lack natural ECM components to promote cell growth, and display loss of mechanical properties and leaching of toxic diluents/products upon degradation [4, 11, 19]. Due to this, natural polymers present a potentially more desirable route of processing because of their inherent ECM characteristics and bioactivity.

1.3.4 Material Heterogeneity: Natural Polymers

Natural polymers such as alginate, chitosan, hyaluronic acid, collagen, and gelatin have already been modified for 3D tissue engineering applications [2, 4, 6, 8]. However, many natural polymers have few µSL applications and require either co-polymerization with a synthetic polymer or reaction with synthetic chemicals to achieve photoactive properties. Natural polymers can be reacted with chemicals like methacrylic anhydride to modify the structure and add acrylate groups to the polymeric backbone. Typical photocrosslinkable modifications of natural polymers require di-acrylates, methacrylates, or acrylamides to be added in as side groups. Various degrees of modification of natural polymers have been reported, typically ranging from as low as 10% to as high as 99% [11, 24, 25]. However, not all natural polymers are used for µSL applications, so having a photoactive element does not mean the material will be compatible with µSL. This can depend on the degree of modification, wavelength of light, and µSL system being used to produce the desired structure. The most common natural polymers that will be discussed for this work include: alginate, chitosan, hyaluronic acid, collagen, and gelatin.

Alginate is a naturally occurring polysaccharide found in the cell walls of brown algae [26]. Alginate has been previously printed using extrusion-based and laser assisted methods, with reports that it is a biodegradable material with no inflammatory response. However, alginate lacks cell adhesion ligands for cell attachment [2]. In µSL, oxidized methacrylic alginate (OMA) scaffolds have been functionalized with Arginine, Glycine, and Aspartate (Arg-Gly-Asp, or RGD) sequences to promote cell adhesion and co-polymerized with synthetic poly(ethylene glycol) methyl ether methacrylate (PEGMEM) to improve degradation and printing [27]. Utilizing RGD to improve cell adhesion is common with synthetic or non-cell-adhesive natural

polymers. RGD is an amino acid sequence found in ECM proteins and act to help simulate and mimic the ECM environment *in vivo* – more specially, cell membrane proteins known as integrins act as receptors for RGD sequences, recognizing their ligands and binding with the sequences to mediate cell-cell attachment and interactions [4, 5, 7]. The resulting µSL alginate scaffolds had mechanical properties suited for musculoskeletal and cartilage applications [28]. Although this is an incredible feat in the realm of tissue engineering, the necessity of synthetic polymers and functionalization with RGD sequences still creates drawbacks when considering the biodegradability and biocompatibility of the resulting tissue scaffolds.

Chitosan is another polysaccharide (sugar) composed of D-glucosamine and *N*-acetyl-D-glucosamine, and is commonly extracted from the exoskeleton of crustaceans and insects [26]. Chitosan has also been utilized in extrusion-based printing, but with limited cell viability (~75%) [2, 5]. For µSL chitosan has been hybridized with PEGDA in order to create ear-shaped scaffolds with 50 µm pore sizes for cartilage regeneration [29]. Once again, since chitosan is a natural polymer it mimics ECM characteristics in order to promote cell growth. PEGDA was chosen for its ease of processing with µSL. However, as expected the presence of PEGDA limited the biocompatibility and biodegradability of the scaffold and increased the mechanical strength/rigidity of the resulting scaffolds [29]. Although, chitosan is inherently biodegradable so it promotes degradability within the scaffold with the limitation of non-degradable PEGDA.

Hyaluronic acid (HA) is also another polysaccharide. Additionally known as hyaluronan, HA is a glycosaminoglycan (GAG) found in mammalian tissues (particularly mammalian connective tissue: cartilage, ligaments, and tendons) [26, 28]. GAGs are long chains of disaccharide units

with side groups that link collagens to form a network of ECM [26]. This characteristic of HA is what makes it a potentially attractive biomaterial for use in µSL. Unlike alginate and chitosan, the µSL applications of HA have been explored more extensively [list refs here]. Suri *et al* reacted HA with glycidyl methacrylate to produce GMHA, a photoactive HA due to the added methacrylate groups [30]. Although no mechanical data was reported, tubular "nerve guides" were created using a µSL technique. Even though HA is a biomaterial it is not inherently cell adhesive and the resulting GMHA was modified with cell-adhesive peptides and proteins to promote cell growth. Other HA µSL feats included co-polymerizing HA with PEG [28]. The addition of PEG increased the mechanical strength of the scaffolds, which were then intended for cartilage repair [28].

Lastly, collagen, and its derivative gelatin, is one of the most widely used natural polymers in regenerative medicine and tissue engineering [2, 4, 28]. Collagen is a part of the ECM and is found in both hard and soft connective tissues, as it makes up 20-30% of the protein in mammalian bodies [2, 5]. Collagen chains contain RGD residues that allow for cell-adhesion [2, 6, 26]. In addition, collagen is also biodegradable via the body's natural enzymes [2]. Collagen and gelatin contain enzymatic sites which matrix metalloproteinases (MMPs) can cleave and allow for further expansion and proliferation of cells throughout the body [2]. What makes collagen different than the previously mentioned natural polymers is its versatility. Collagen's mechanical properties are generally suited for wound-healing applications (particularly skin) and other soft tissues unlike chitosan and HA which are generally used for cartilage repair [28]. This makes collagen a versatile material in that it can be combined with other natural polymers like HA to increase mechanical strength and enhance biocompatibility in harder tissue applications

[28]. Although almost all bio-AM utilizing collagen is extrusion-based or laser assisted, gelatin (which is partially denatured collagen), can be used in SL and µSL applications [2, 5, 11, 31]. Gelatin is water soluble and forms physically crosslinked gels below 35°C. Although these gels are not stable at physiological temperatures (37 °C), gelatin can be chemically crosslinked upon modification to become thermally stable for bio-AM applications [5].

1.3.5 Biocompatibility and Cell-Material Interactions

When designing a tissue engineering and biomaterial scaffold, the intention is cells will populate the scaffold and the body's natural regeneration mechanisms will take over [7, 23]. In doing so it is important to understand that cells depend on the diffusion of nutrients and waste to survive. In the human body, the average inter-capillary distance is around 100 µm in order to support diffusion of nutrients and waste in tissues [9]. It is also important to consider the average size of a eukaryotic cell is around 25 µm, but mammalian cell sizes can range anywhere from 5-100 µm [32]. Thus, being able to produce a 3D tissue engineering scaffold that mimics these natural parameters would be ideal, and research regarding cell-scaffold interactions in 3D is pioneering [4, 7, 11, 12, 23, 31]. What research has shown so far is 3D tissue scaffolds should aim to imitate the ECM *in vivo* [7, 12, 31]. The ECM is a complex, heterogeneous network of structural proteins and signaling molecules arranged in a 3D manner to provide structural support to living cells. [12, 31]. Understanding the cellular microenvironment has become pivotal in understanding how to enact the body's natural regenerative processes (wound healing, tissue/organ growth); and, developing 3D tissue engineering scaffolds is crucial to continue this research [11, 12, 23, 31].

1.4 Gelatin and Gelatin Methacrylate

Gelatin is a natural biopolymer derived from collagen, making gelatin and any of its modifications of particular interest for biomaterial development. GelMA (referred to in the literature as methacrylated gelatin (MeGel), methacrylamide modified gelatin, gelatin methacrylamide, or gelatin methacrylol as well) is a biocompatible and biodegradable polymer that undergoes free radical polymerization in the presence of a photoinitiator and UV light to create a hydrogel network [25, 28, 33]. Once crosslinked, GelMA is thermally stable at and above physiological temperatures [25]. Being a derivative of collagen, GelMA contains RGD sequences to support cell-adhesion and MMP sites to promote enzymatic degradation [25]. This means GelMA does not require further functionalization with cell-adhesive ligands or proteins like alginate or HA. Additionally, since GelMA is not co-polymerized (although it can be) with PEG, the degradability and strength of resulting photocrosslinked hydrogels is not effected unlike chitosan. The strength of GelMA hydrogels can instead be altered by increasing or decreasing the concentration of a GelMA in solution, or varying the degree of modification of GelMA during the synthesis [34]. The biocompatible, biodegradable, and mechanical properties of GelMA have made it stand out among synthetic and natural polymers. However, the majority of research conducted this far has been in drug delivery, micro-fluidics, cell-encapsulation, soft lithography, and extrusion-based printing [25, 33, 35]. While GelMA has been utilized in µSL applications, there is a gap in the literature in what qualifies GelMA 3D printing. This is because 3D printing of GelMA with SL or µSL techniques has not shown high complexity in the z-direction of printing. However, before delving into this gap in the literature, a few more of the basics of GelMA will be covered including: GelMA synthesis, µSL resin development, and photoinitiator concerns. All of these categories are relevant to the gap in the z-direction because

they impact the reactivity and characterization of the result GelMA resins to be tested. Researchers have been grappling with modifications to GelMA itself, modification to the GelMA resin produced, and concerns with crosslinkers and photoinitiators that ultimately affect the fidelity of a 3D print. This has led to less complex "3D" scaffolds in terms of their z-height that needs to be addressed and improved upon with GelMA and μSL applications.

1.4.1 Synthesis of GelMA

GelMA undergoes a facile synthesis in which gelatin is combined with methacrylic anhydride (MA) in water or phosphate buffered saline (PBS) at 50°C [24, 35]. During this process the MA monomers are reacted with the lysine and hydroxyl lysine side groups on the gelatin backbone (Figure 1-3) [24]. This synthesis is commonly referred to as a "one-pot" synthesis, and was originally developed by *Van Den Buckle* et al in 2000 (and has remained unchanged) [36].

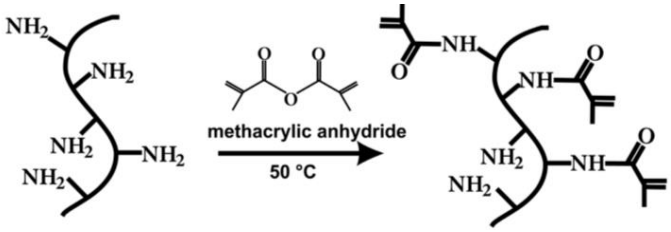

Figure 1-3. GelMA Synthesis Scheme. Figure reproduced with publisher's permission [35].

To confirm the resulting GelMA product HNMR is used (Figure 1-4). The reduction in peak a, and appearance in peaks b, c, and d correspond to GelMA. One interesting property of the synthesis of GelMA researchers may control is the percentage of methacrylate side groups per volume. This is known as the degree of functionalization (DF), substitution (DS), or methacrylation (DM) and can be quantified via colorimetric assays or HNMR [24, 34, 35]. Most batches of synthesized GelMA range between a DS of 20 ~ 80%, however, Shirahama *et al* has recently improved the GelMA synthesis to consistently obtain DM over 90% [35]. A higher DS

correlates to faster curing and higher mechanical strength GelMA [34-36]. Another way to increase the curing kinetics and mechanical strength of GelMA is to increase the w/w or w/v percentage of GelMA in solution. A higher concentration of GelMA also correlates to faster curing and higher mechanical strength/moduli [36]. The exploration of various GelMA solutions, or resins, for use in µSL has allowed for potential expansion of the repertoire of printable biocompatible µSL materials, and for further understanding of 3D tissue engineering environments.

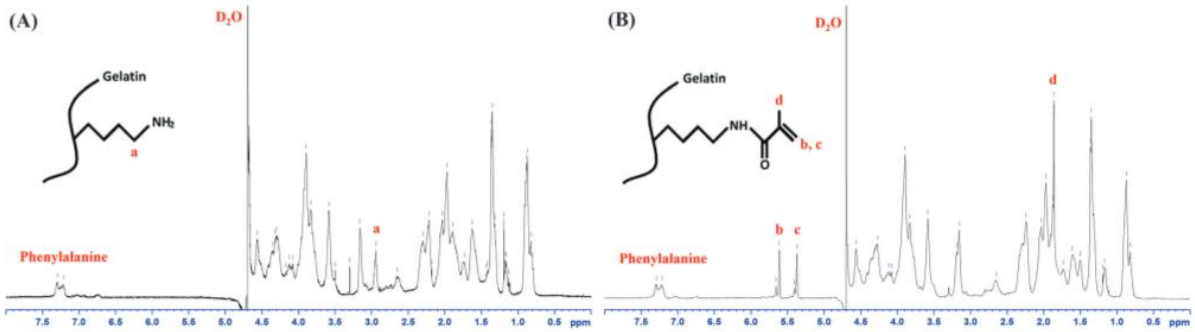

Figure 1-4. (A) HNMR of gelatin. (B) HNMR of GelMA. Figure reproduced with publisher's permission [37].

1.4.2 Development of a µSL resin

To create a photocurable resin for µSL generally requires five components: a monomer with photoactive side groups, a solvent to form the solution/resin, a photoinitiator to initiate the crosslinking reaction, a photoabsorber (also known as a UV blocker) to aid in controlling layer thickness/scaffold resolution, and any additional components required to alter the resulting resin's characteristics (such as diluents to reduce resin viscosity) [3, 9, 11, 14, 15]. With GelMA, a common photocurable resin consists of: GelMA, water or phosphate buffered saline (PBS, solvent), and Irgacure 2959 (photoinitiator) [25, 33, 35]. The curing mechanism behind this type of GelMA resin is shown in Figure 1-5. The reaction is known as free-radical polymerization, where an intermediate is created by irradiation of the photoinitiator and crosslinking follows [3].

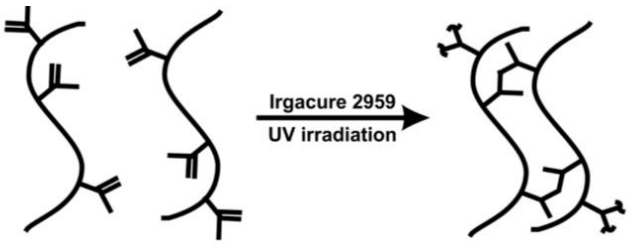

Figure 1-5. Crosslinking of GelMA in the presence of UV irradiation, Irgacure 2959 and PBS to create a hydrogel network. Figure reproduced with publisher's permission [35].

If the monomer itself is not already one biocompatible concern, then developing a biomaterial that is soluble with a photoinitiator, UV blocker, and any additional components can add additional challenges. Diluents combined with natural photopolymers have led to toxic by-products upon leaching or degradation. The selection of resin components is crucial for processing with µSL. GelMA has already been established as a viable biomaterial, but photoinitiators and UV blockers are synthetic materials that can introduce toxicity when trying to use GelMA in bio-AM applications.

In µSL, common sources of toxicity that can reduce a resin's biocompatibility include: trapped unreacted monomer (after crosslinking), residual photoinitiator, residual UV blocker, residual solvent (if organic and cytotoxic), high concentrations of photoinitator, high concentrations of UV blocker, and byproducts of polymer degradation [11, 28]. Balancing all of these components is critical to developing a successful µSL resin. Using GelMA, PBS, and Irgacure 2959 as an example of how these components influence the resulting resin, one might experience the following scenarios: if there is too much PBS, the methacrylate volume would be reduced and the resin might not cure… increasing the amount of GelMA is an option, but then the resin viscosity would increase and the resin could not be processed using µSL… adding more Irgacure 2959 might reduce the crosslinking time, but might cure a thicker layer of material, and could

reduce the resulting scaffold's biocompatibility due to leaching of unreacted Irgacure 2959 or unreacted monomer since the total crosslinking is not 100%… and lastly, a UV blocker could be introduced to reduce layer thickness, but since it absorbs UV irradiation it would slow down the crosslinking process and potentially introduce a toxic element to the resulting scaffold.

1.4.3 Additional Printability Considerations: The Photoinitiator

Of all of these components the one that garners the most concern is the photoinitiator [28]. This is because, photoinitiators are inherently cytotoxic and they tend to be non-water soluble [28]. There are ways to combat this issue, particularly a wide variety of photoinitiators are available for µSL applications, but each photoinitiator has its advantages and disadvantages. With GelMA and µSL, the following photoinitiators have either been used, or are worth mentioning for the purposes of this research: 2-hydroxy-l-[4-(hydroxyethoxy)phenyl]-2-methyl-l-propanone (Irgacure 2959), 2,2-dimethoxy-2-phenylacetophenone (Irgacure 651, DMPA), lithium phenyl-2,4,6-trimethylbenzoylphosphinate (LAP), 2,2'-Azobis[2-methyl-N-(2-hydroxyethyl) propionamide] (VA-086), and Eosin Y/Triethanolamine/l-vinyl-2-pyrrolidinone (EY) [28, 38].

The choice of photoinitiator tends to come down to two things: the light source being utilized on the µSL apparatus (the wavelength required for the photoinitator to release an intermediate for the crosslinking reaction to occur) and the solvent to dissolve the photoinitiator. Of course, the biocompatibility of the photoinitiator is important as well because even though photoinitiators are cytotoxic, some are less toxic than others [28]. Irgacure 2959 is one of the most common photoinitiators and is used in almost every photocuring application of GelMA [25, 28, 33, 35, 36]. This is due to it being the least cytotoxic of the family of Irgacures and is water soluble [28,

38, 39]. However, most applications with GelMA and Irgacure 2959 are better suited for 2D applications such as biopatterning and microfluidics [40-42] as Irgacure 2959 is considered a "weak" photoinitiator with a broad absorbance spectrum and long exposure times compared to other photoinitiators [25, 43, 44]. This is acceptable for 2D applications because the thickness of the resulting components is generally less than 1 mm and the resulting components do not require complex pore shapes or sizes. For example, Kolesky *et al* utilized extrusion-based printing with GelMA, Irgacure 2959, and PBS to create 2D vascular constructs for various cell types [41]. The scaffolds produced by Kolesky mimicked vasculature and some microfluidic device applications, and in the XY direction were greater than 2 mm, however, no analysis on the z-direction was reported. Also, no fidelity analysis of the filament extrusion or deviation from .STL or CAD file was reported. Only few representative images of scaffolds were shown, without any further fidelity quantification. Additionally, they claim to use this same resin to create a heterogeneous 3D tissue construct, but from their images the height of each scaffold is less than 1 mm. Due to the limitations of their extrusion-based printer, the pore sizes of the resulting tissue constructs were 200 μm (however, for their desired application this was sufficient). Bertassoni *et al* also utilized GelMA, Irgacure 2959, and PBS for extrusion based printing of HepG2 (liver cells) and NIH3T3 (skin cells) bioinks to create "3D" architectures [42]. Cell viability was sufficient, but the paper does not show side or isometric views of their resulting architecture, so a z-dimension is missing, and their scaffold pore size was 500 μm. The cure times of their constructs averaged around 60 s. If μSL was used, a potentially more complex structure could be manufactured with a low cure time and 3D shape with a z-dimension greater than 1 mm. While the use of Irgacure 2959 in μSL has not proved to be entirely viable, it has produced 3D scaffolds with heights higher than 1 mm. Ovsianikov *et al* demonstrated this with

their two photon printing (2PP) of GelMA (they refer to it as GelMOD), Irgacure 2959, and PBS resin [44]. 2PP is a type of µSL that utilizes a single laser that rasters across the resin instead of a projecting each layer with a dynamic mask [44]. The 2PP apparatus used emitted light at 515 nm, and Irgacure 2959's wavelength is close to the half-wavelength emitted by that source, making it a suitable choice for their setup. The authors were able to successfully cure ~2.5 mm tall scaffolds. Printing one scaffold took 5 hours and no quantification of fidelity in comparison to the intended CAD file was reported. Although a perceivable 3D scaffold was produced, the pore size and architecture did not fully display the capabilities of µSL, and could be theoretically produced using extrusion-based techniques. Also, 5 hours to produce one scaffold is an incredibly long time especially considering the scaffolds were nearly 3 mm tall. However, the authors were able to successfully adhere bone cells to the scaffolds to demonstrate its biocompatibility. Irgacure 2959 is definitely a good choice of photoinitiator for GelMA applications, but might be best suited for 2D applications due to its limitations in photoactivity and cure time. Testing alternative photoinitiators is an option to overcome these limitations.

DMPA is another photoinitiator with 3D printing and bio-AM applications [3, 28, 38, 45, 46]. DMPA has wavelength peaks at 240 and 350 nm, is non-water soluble, and more cytotoxic than Irgacure 2959 [28, 38, 39]. Due to its insolubility in water and cytotoxicity, DMPA tends to be used with synthetic polymers instead of natural ones, but has been used with GelMA [45-48]. However, not all of these applications were µSL based. A purely synthetic example was demonstrated Chan-Park *et al* [48]. In this paper, novel diacrylated triblock macromers were produced and micropatterned using soft photolithography. This lithography technique is similar to µSL, but a 3D construct is not produced, thus it is a 2D approach. However, from this the

authors noted that cure times of their novel macromers with DMPA ranged from 7-56 s. This fast cure time is already a huge improvement over Irgacure 2959. Additionally, the authors proved cell-adhesion to some of their novel macromers after rinsing them with acetone to remove any remaining uncured macromer, immersing the samples in a 70:30 ethanol water solution for 3 days, and then rinsing the samples with PBS before proceeding to cell culture. These washing steps were necessary to rid the samples from any unreacted or residual toxic components and promote the idea that although DMPA may be more cytotoxic than Irgacure 2959, it still has shown cell viability. Chartrain *et al* displayed the use of DMPA with a biodegradable photocurable polyester using µSL [47]. The resulting 3D scaffolds had larger pore sizes (400 x 800 µm), but 7.5 s cure times per 100 µm layer with the inclusion of a UV blocker in the printing resin. The paper also showed the exclusion of the UV blocker ended up in the pores filling up, i.e. a reduction in print resolution, but a faster cure time of 1.5 s per 100 µm layer. Additionally, a 1 day cell culture study demonstrated the printed material had higher viability than tissue-culture treated polystyrene with a 2 w/w % concentration of DMPA. The fast cure time of DMPA makes it an incredibly attractive photoinitiator for µSL applications, however its water insolubility is its biggest drawback. Because of this, DMPA must be dissolved with harsh organic solvents like acetone or NVP, which introduce a toxic component to the printing resin [39, 46, 48]. The water insolubility of DMPA also makes µSL applications with GelMA and DMPA almost non-existent since harsher solvents like isopropyl alcohol or acetone are used to dissolve DMPA alternatively, and gelatin will precipitate in these solvents [49]. Kim *et al* used SL with a 365 nm light source to make poly(ethylene glycol) dimethacrylate (PEGDMA) and GelMA nanopatterned cell culture substrates to model a vascular environment [45]. Although this is a 2D application of GelMA with DMPA, their results showed tunable mechanical, cell-

adhesive, and degradation properties of the cured patterns based on GelMA and PEGDMA concentrations. Skardal *et al* utilized methacrylated hyaluronic acid (HAMA) and GelMA (which they refer to as GEMA) to create a HAMA-GEMA bioink for use in extrusion-based printing [46]. The results showed the resulting resin supported the growth of HepG2 and NIH3T3 cells and did not initiate an inflammatory response when injected under the skin of nude mice. The authors also produced a "3D" tubular structure, but the paper does not depict the height of the desired shape. The authors admit the structure lacks complexity and could be improved upon, but demonstrated the potential viability of this bioink for AM applications. DMPA definitely has its advantages and disadvantages over Irgacure 2959, and could show future adaptions in µSL of GelMA.

Of the remaining photoinitiatiors mentioned, LAP and EY have all shown SL techniques with GelMA, while VA-086 has only shown 2D micropatterning with LED light [43, 50-53]. However, from the "3D" printing works, a gap still remains in the literature of what constitutes a true 3D printed scaffold. Fairbanks *et al* used LAP in comparison with Irgacure 2959 to create PEGDA hydrogels using a 365 nm light source [43]. Their results revealed solutions with LAP had a cure time that was 1/10 of those with Irgacure 2959. This demonstrated LAP's advantages over Irgacure 2959 as a more efficient photoinitiator that is also biocompatible and water soluble [28, 38]. However, the resulting hydrogels were still 2D films. PEGDA was also studied with the addition of cellulose nanocrystals (CNCs) in a µSL system with LAP in order to increase the mechanical properties of PEGDA scaffolds [54]. In this applications the authors were able to produce high complexity "butterfly" scaffolds and even a reproduction of a human ear, the 3D printing fidelity was definitely displayed but the authors included no biocompatibility studies

regarding their resulting printing resin [54]. However, both of these µSL applications with LAP were demonstrated with PEGDA, not GelMA. There is room for expansion and exploration of GelMA LAP photocureable resins with µSL applications.

Taller structures with GelMA and LAP in µSL have yet to be reported on. Most applications are in micropatterning or 2D SL, not µSL fabrication. One example comes from Monteiro *et al*, these researchers explored the use of LAP over Irgacure 2959 in dental applications of GelMA. The authors showed that LAP exhibited less cytotoxicity compared to Irgacure 2959 when cured with a dental light due to the differences in the absorption peaks of the photoinitiators [55]. Additionally, the authors note increasing the concentration of LAP increased the cytotoxicity of the GelMA resin. However, in Monteiro *et al* no 3D scaffold or structure was produced, thus LAP could further be studied in µSL to expand the literature regarding 3D printing GelMA. EY was also tested as a water soluble photoinitiator that is less cytotoxic than Irgacure 2959 and has a peak wavelength at 514 nm [28, 38, 50, 51]. In their Master's thesis, Wang set out to create a novel photocurable resin to be 3D printed using a visible light µSL system and printing resins of GelMA-PEGDA and GelMA with EY as the photoinitiator [50]. The GelMA-PEGDA resin exhibited higher mechanical properties but less cell adhesion than the GelMA resin. The resulting scaffold produced, however, did not display a high resolution. Instead a simple lattice structure was produced with 1 cm square pores, and did not contain a z-axis measurement or fidelity analysis. In another recent Master's thesis McColl set out to do the same thing as Wang experienced similar results [51]. The resin McColl used was nearly identical to that of Wang and so was the visible-light based µSL system. However, McColl strictly focused on 3D printing a resin with GelMA, and admitted that their produced scaffolds did not significantly improve upon

current GelMA 3D printing. McColl was unable to provide any images indicating the z-height of their scaffolds, but claimed their scaffolds were less than 2 mm tall. Additionally, the resin cure time ranged from 60-120 s using EY. Both McColl and Wang did not analyze the fidelity of their prints produced, or measured any tolerances of their µSL system.

Lastly, since µSL applications with VA-086 and GelMA cannot be found, it is not the most viable photoinitiator for this application. Billiet *et al* demonstrated extrusion-based printing of GelMA with VA-086 as a photoinitiator [56]. The resulting scaffolds ranged from 1 ~ 3 mm in height. Much like Ovsianikov *et al* demonstrated "tall" scaffolds of GelMA with Irgacure 2959, the resolution limits of the printing technique or resin prevent any demonstration of highly complex GelMA scaffolds. However, the authors of Billiet *et al* were still able to create a 3D construct using GelMA and VA-086 that exhibited cell viability with HepG2 cells which is a feat in itself. As far as the literature is concerned, a representation of µSL printing GelMA scaffolds greater than 2 mm in height, with a quantifiable comparison to the intended CAD or .STL file does not exist. This section has outlined numerous attempts utilizing various types of photoinitiators, which was a key consideration for µSL GelMA material development.

1.5 Thesis Aims

The overall goal of this work is to develop a novel GelMA resin that will improve on the previously discussed µSL applications of GelMA. Improvements would mainly be defined as a reduction in cure time, increase in scaffold height, and increased scaffold geometry/resolution displayed in the literature. Additionally, providing a quantifiable method to characterize print

fidelity in μSL is a concern. Since GelMA is regarded as a biocompatible material, the biocompatibility of the resulting resin will be assessed but is not a main concern. These improvements are broken down into the following specific aims:

1. Develop a novel GelMA resin that can print a 3D scaffold with a height greater than 2 mm. This resin should also improve on the overall cure time of the scaffold produced.
2. Display the complexity of μSL with this novel GelMA resin by being able to produce a scaffold with porosity and pore sizes less than 500 μm, and a layer thickness less than 200 μm

In order to address the first aim, the literature has shown a variety of GelMA compositions. Some compositions include additional monomers like PEGDA to improve printability, or UV absorbers to improve feature sizes. Ideally a resin containing only GelMA would display an improvement on current resins in the literature, but other monomers may be explored as this approach is common. Additionally, it is clear from the literature Irgacure 2959 is not the most efficient photoinitiator. Although a 3D scaffold of GelMA has been produced with Irgacure 2959, it took 5 hours to produce. A resin that can incorporate DMPA or LAP as the photoinitiator should demonstrate a lower cure time. The immediate issue with using DMPA is that it is not water soluble so other solvents for GelMA and DMPA may have to be explored. To measure the first aim the following techniques will be employed: optical microscopy, photo-rheology, photo-DSC (differential scanning calorimetry). Optical microscopy will be used to measure scaffold height and printed feature sizes. Photo-rheology is a technique that measures the storage modulus over time of a material as it cures under UV exposure. Photo-rheology provides insight into the viscoelastic properties and cure time of the resin. The time (in seconds) it takes the modulus of stiffness (G') to reach constant value, indicates the cure time. Photo-DSC

is another valuable technique that provides insight into the cure time and curing kinetics of the resin. Photo-DSC measures the heat of reaction of the resin over time, and produces a peak once the resin has fully cured. The time in which this peak occurs corresponds to the cure time. The area underneath the curve can be measured to quantify the specific heat of the material. Typically, a large exotherm would correspond to a very reactive resin [57]. A working curve will be developed to determine the layer thickness and exposure time of the material for the printing process. A working curve plots the layer thickness as a function of UV exposure. To measure this, a thin layer of resin may be cured at the surface for a specified amount of time and then measured using a micrometer to determine its thickness. In altering the exposure, varying thickness measurements can be taken and a plot can be developed. This plot gives insight into what type of layer thickness can be expected from a print as well as proving insight into what type of exposure time would generate a certain layer thickness. Developing a working curve is necessary for both aims 1 and 2.

To address the second aim: the literature thus far has not provided a GelMA containing scaffold with layers less than 200 µm. Although porous 3D GelMA scaffolds have been produced with extrusion, with µSL the porous structures produced are not 3D and do not display heights greater than 2 mm. These marginal values provide a good baseline for an improvement on the literature, and would potentially provide researchers insight on how µSLA feature sizes can be tailored. In order to reduce the layer thickness or increase the resolution of the 3D scaffold, it is likely that a UV blocker will be incorporated into the resin. Ideally the UV blocker would be water soluble and non-toxic to cells. To measure the pore size and layer thickness, and quantity print fidelity, optical microscopy will be used. Optical microscopy can measure the feature sizes immediately

after a scaffold is produced. Though it may not be as precise as scanning electron microscopy (SEM), it is more accessible and SEM has been deemed outside the scope and scale of this work.

Beyond these aims, additional characterization techniques will be employed in characterize the properties and performance of the developed GelMA resin. Swell testing will be necessary to understand the water content and hydrogel properties of the resulting resin. Cell studies will be performed to measure the biocompatibility of the cured resin and observe any cytotoxic response.

The importance of μSL is it can fabricate complex scaffolds with feature sizes similar to *in vivo* cellular environments, but lacks a repertoire of biomaterials to do so. Potential applications for high resolution scaffolds include: precise anatomical models for pre-surgical planning, wound healing (skin substitutes), organ regeneration, and drug delivery [11]. GelMA has already been identified as a biocompatible and biodegradable photocurable material, making it an ideal candidate to increase the current repertoire of synthetic and natural available μSL materials. Quantifying and characterizing a novel photocureable GelMA resin is a necessary and significant contribution to current work that has yet to report structures greater than 2 mm in height and measure the fidelity and repeatability of printed scaffolds.

Chapter 2: Materials and Methods

Based upon the previous literature review (Chapter 1), several resins were explored before choosing GelMA as the focus of this research. Appendix A outlines these other resins. In general, the GelMA resin was developed in the following way:

1. GelMA synthesis and characterization via nuclear magnetic resonance (NMR) spectroscopy,
2. Photo-curable resin formulation development, photo-rheology, photo-Differential Scanning Calorimetry (DSC),
3. Cured film fabrication and swell-testing,
4. 3D Printing development with working curve, 3D printing and optical microscopy analysis
5. Cell culture.

Photo-DSC and photo-rheology are relatively new, thus these techniques are not currently reported often. The authors believe this type of instrumentation would offer additional insight into the resin development and so it was decided to utilize these tools in order to further characterize the photo-curable system as well as adding to the repertoire of printability analyses available in literature.

2.1 Materials

The following materials for this work were purchased from Sigma Aldrich and distributed from the United Sates: GelMA was produced from type B gelatin (200 bloom), and methacrylic anhydride (MA); NMR was performed on GelMA using deuterium oxide (D_2O) (99 atom %); GelMA films and 3D prints were cured with 2-Hydroxy-4-methoxybenzophenone-5-sulfonic acid (sulisobenzone, UV blocker) and Lithium phenyl-2,4,6-trimethylbenzoylphosphinate (LAP, photoinitator); Mouse fibroblasts, NIH/3T3, ATCC® CRL-1658™ were cultured in α-MEM supplemented with 10% fetal bovine serum (FBS), 1% penicillin streptomycin, and amphotericin B and cleaved with trypsin-EDTA (0.5%). The following materials were purchase from Gibco Sciences (USA): phosphate buffered saline (PBS) was used to make GelMA as well as culture cells. The following materials were purchased from Thermo Fischer and distributed in the United States: dialysis was performed on GelMA with SpectraPOR 4 dialysis tubing (12-14 kD MWCO, 75 mm Flat-width) and deionized (DI) water. Trypan blue was used to count cells and qualify viability, while 4′,6-diamidino-2-phenylindole (DAPI) and Texas Red sulfonyl chloride were used to stain GelMA films post cell studies for confocal imaging (Thermo Fischer, US). Lastly the [3-(4,5-dimethylthiazol-2-yl)-5-(3-carboxymethoxyphenyl)-2-(4-sulfophenyl)-2H-tetrazolium (MTS) assay was used to quantify cells for proliferation and mitochondrial activity and purchased from Promega (USA). All chemicals were used as purchased with no further purification.

2.2 Gelatin Modification and Verification

2.2.1 Gelatin Methacrylation

Gelatin was modified by adapting previously published protocols [25, 33, 35, 42]. Briefly, 10 g gelatin was dissolved in 80 mL PBS on a hot plate with rapid stirring at 60 °C. Once the gelatin was fully dissolved, 20 mL MA was added and stirred vigorously at 1300 rpm. The temperature and stirring were maintained overnight to allow for complete reaction. The following day the solution was moved to dialysis tubing and placed in excess DI water with stirring at 150 rpm. The dialysis water was changed 3 times on the first day, and twice every day thereafter until the solution appeared clear/pale-amber in color (4 – 7 d). After the solution was dialyzed, it was centrifuged at 1500 rpm for 10 min and the supernatant was collected. The resulting GelMA solution was then frozen overnight at -4°C and lyophilized the following day for 3 d to yield a purified white foam-powder. The GelMA product was stored in a freezer at -80°C with desiccant for future use.

2.2.2 NMR Spectroscopy

1H NMR (500 MHz Prodigy, Bruker, US) was used to determine the degree of methacrylation (DM) of GelMA (also referred to as the degree of substitution, DS). First, 50 mg GelMA was dissolved in 1 mL 99 atom % D_2O at 40 °C. 1 H NMR was performed at 64 cycles and 400 MHz. Plain gelatin was run for a control. From the resulting spectra the degree of methacrylation was determined by integrating the GelMA spectrum at 2.9 ppm (lysine methylene signal) after normalizing the GelMA spectrum with respect to the plain gelatin using the phenylalanine peak at 7.2 ppm. Next, the area was integrated from 7.0 – 7.5 ppm (phenylalanine), then the lysine

methylene signal was integrated from 2.85 – 2.95 ppm. The reduction in the peak at 2.9 ppm corresponds to the degree of methacrylation [25, 35]. Gelatin modification can also be confirmed by the appearance of methacrylic functional groups at 5.4 and 5.6 ppm, in addition to the appearance of a methyl functional group at 1.9 ppm. The following equation was used to calculate the degree of methacrylation (where DS refers to degree of substitution, an A refers to the area beneath the peak from the NMR spectra):

$$\mathrm{DS} = \left(1 - \frac{A(\text{lysine methylene of GelMA})}{A(\text{lysine methylene of gelatin})}\right) \times 100\% \qquad \text{(Equation 2-1) [37]}$$

2.3 Photo-curable Resin Formulation

Each GelMA resin shown in Table 2.1 was created by a weight by weight (w/w %) measurement of the starting polymer (GelMA) to the total solvent weight (DI water). For example, a 10 mL printing resin of 20% GelMA with 0.5% sulisobenzone would consist of the following: 8 g DI water, 2 g GelMA, 0.05 g sulisobenzone and 0.05 g LAP. For all GelMA resins, the concentration of LAP was held at 0.5%. The 3D print resins were produced by first dissolving the sulisobenzone and LAP in DI water (stirred at 40 °C). Then, the respective GelMA amount was added to the beaker. The beaker was covered in Parafilm® and stirring was reduced to 60 rpm until the solution was a uniform amber color with no bubbles (approx. 1 hr.).

Table 2-1: GelMA resin formulations

	GelMA (w/w %)	Sulisobenzone (w/w %)	LAP (w/w %)
L-GelMA 1	10.0	0.5	0.5
L-GelMA 2	10.0	1.0	0.5
M-GelMA 1	20.0	0.5	0.5
M-GelMA 2	20.0	1.0	0.5
H-GelMA 1	30.0	0.5	0.5
H-GelMA 2	30.0	1.0	0.5

2.3.1 Photo-Rheology

A TA Instruments Discovery Hybrid Rheometer with a UV Source attachment was utilized to perform photo-rheology on GelMA resins at 22 ℃. A parallel plate setup was used and GelMA resins were pipetted directly onto the quartz crystal surface of the rheometer, any excess material was removed once the gap was closed. The experiment was setup with a 30 s delay in which the shutter was closed. After 30 s the shutter opened to expose the resin to a light intensity of 9 mW/cm^2 (the minimum intensity of the UV light source). The light intensity was confirmed before the experiment using an irradiance meter. Samples were run at a strain of 0.3% and frequency of 2.0 Hz. The total time of each experiment was 300 s. The same light source used for photo-rheology was also used for photo-DSC (OmniCure® Series 2000). The experimental procedure was adapted and referenced from Golaz *et al* 2012 [57].

2.3.2 Photo-DSC

A TA Instruments Discovery DSC with a photocalorimeter accessory (PCA) was utilized to perform photo-DSC on GelMA resins at room temperature. Using Tzero DSC pans, 15 – 20 mg GelMA resins samples were tested. First an isotherm was set for 1 min at 20 ℃ prior to the shutter opening. The experiment proceeded for 3 min after which the shutter was closed and an additional isotherm at (20 ℃) proceeded prior to ending data collection. The experimental procedure was adapted and referenced from Golaz *et al* 2012 [57].

2.4 Film Fabrication and Swelling

2.4.1 Film curing

To create films for use in swell testing and cell culture studies a silicone casting mold was used. The silicone mold consisted of three pieces: a top flat layer, a middle layer with multiple punches of 14 mm diameter discs, and a bottom flat layer. Each resin was pipetted into the mold until it filled the perimeter (approx. 250 μL). Then, the top sheet was rolled over the film to ensure no bubbles were present and the disc was flat on both sides. A 365 nm UV lamp (OmniCure® UV LED head, 15W/cm^2) was used to cure the films for 30 s on each side. After cured, the top and middle layers of the mold were removed to reveal films approximately 14 mm in diameter and 1 mm in thickness.

2.4.2 Swell Testing

Swell testing was performed on all GelMA films. The films were weighed immediately after fabrication to obtain their bulk weight. A micrometer and caliper were also used to determine their average thickness and diameter. The films were then submerged in PBS and allowed to swell overnight at 22 °C. The swollen weight of the films was then measured. Since the films are more fragile once swollen, their dimensions were not able to be measured wet. After this, the films were then transferred to a petri dish and placed in a vacuum oven at 60 °C for 12 hr to obtain the dry weight. The percentage of water in the films was determined as a function of the swollen weight (W_s) and dry weight (W_d). The following equation was used:

$$\text{Swelling (\%)} = (W_s - W_d) / W_d \times 100\ \% \quad \text{(Equation 2-2) [37].}$$

2.5 3D Printable Resin Validation

2.5.1 Working Curve

A working curve is used to determine the critical exposure (E_c) and depth of penetration (D_p) of photoactive polymer resins [3]. The equation is based on the Beer-Lambert law of absorption and is defined as:

$$C_d = D_p \ln(E / E_c) \text{ (Equation 2-3) [9].}$$

This equation relates the exposure of light delivered at the prepolymer surface (E) to the depth at which the prepolymer is crosslinked, also known as the cure depth (C_d). The minimum exposure required to begin polymer crosslinking is the critical exposure (E_c). The working curve gives insight to the amount of UV energy required for photopolymer curing. Therefore, GelMA resins were exposed to a series of exposure times, ranging from 500 ms to 3000 ms, at the resin surface and then the thickness of the resulting polymer film was measured using a micrometer. The thickness at each exposure was then plotted on a semi-log plot. Typically working curves display a linear relationship between the cure depth and the natural log of exposure. The critical exposure was then determined by the resulting curve's x-intercept. The depth of penetration was determined by the slope of the resulting curve.

2.5.2 Mask Projection Microstereolithography (3D Printing)

An in-house LabView program was developed for the 3D printer and an .STL file of the desired print structure was uploaded to the software prior to printing (Figure 2-1) [9]. The print file was a 4 x 4 x 5 (l, w, h) mm scaffold with 1000 μm pores, where 1-2 mm of the scaffold height was

incorporated as a raft. A raft (also referred to as burn-in layers) is an initial print area (or additional printed section) of a scaffold that is printed in order to improve the overall fidelity of the scaffold. The raft acts similar a sacrificial layer that sets up the printed area on top which will be the true measured printing area. In the case of Figure 2-1, a raft was incorporated as an extra layer of additional pores creating a rectangular shape instead of a square (not shown in Figure 2-1, but an additional row of two 1 mm pores in the x, y, and z planes were incorporated at the bottom of the scaffold).

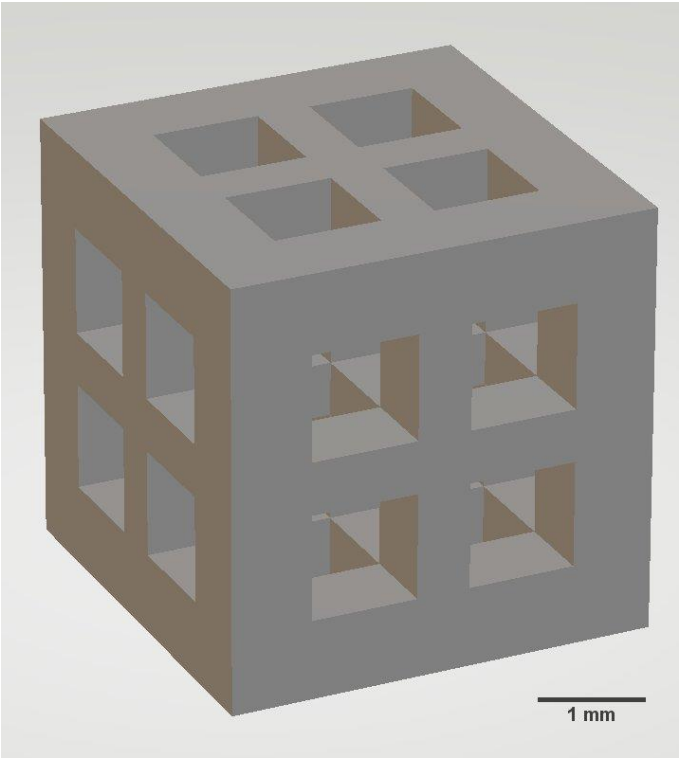

Figure 2-1: Image of the .STL file for desired print structure.

Originally, the intended scaffold design was a scaffold with gradient porosity ranging from 200 µm to 1000 µm sized pores in order to address Aim 2 of this thesis: "Display the complexity of µSL with this novel GelMA resin by being able to produce a scaffold with porosity and pore sizes less than 500 µm, and a layer thickness less than 200 µm." However, preliminary printing discovered this print file could not be printed effectively, nor did the print file retain pore sizes.

The initial printed constructs could not successfully be reproduced, thus a simpler scaffold design (Figure 2-1) was chosen and Aim 2 of this work was adjusted as follows, where the thesis aims are:

1. Develop a novel GelMA resin that can print a 3D scaffold with a height greater than 2 mm. This resin should also improve on the overall cure time of the scaffold produced.
2. Display the complexity of µSL with this novel GelMA resin by being able to produce a scaffold with porosity and pore sizes of 1000 µm, and a layer thickness less than 200 µm

In order to print, 10 mL of GelMA resin was placed into a small beaker and a build stage was attached to the printer then lowered into the resin (see Figure 1.2 for a visual representation of the overall printer). The UV light source (Ushio, Japan) used for printing had an intensity of 10 mW/cm^2. Each layer was cured between 1 ~ 5 s depending on the GelMA resin. The resulting layer thickness was set between 100 and 200 µm. Once the print was finished, it was removed from the build stage and placed into warm water for several minutes to wash out any uncured GelMA resin. The print was shaken lightly and a pipette was used to flush out the porous parts of the structure. After gently washing, the 3D print was blotted with laboratory tissue paper to remove any excess water prior to imaging. The prints were then imaged using an optical microscope (AmScope™ 3.5X-180X Manufacturing 144-LED Zoom Stereo Microscope with 10MP Digital Camera). Isometric and planar images were taken via optical microscopy and the pore size, layer thickness, and overall scaffold dimensions were measured to quantify 3D print fidelity using the AmScope™ desktop software. A print was considered “good” or “bad” depending on how much the pore size and layer thickness deviated from the .STL file of the print. Rather than use qualitative adjectives to define the print, the fidelity was determined based

on a % deviation from the theoretical values of the .STL image (Figure 2-1), reported as the % error. Since no such ranking system or print fidelity analysis currently exists for this particular instrument and resin formulation, a ranking system was developed based off of the instrument's capabilities and/or limitations.

Paul Lambert's thesis (2014), describes an in-depth system characterization which includes tolerances of the designed µSL instrument as well as sources of instrumental error [9]. To validate the developed µSLA printer, he tested a polypropylene glycol diacrylate (PPGDA) photopolymer resin with 2% w/v DMPA as photo initiator and categorized tolerances in the XY, XZ, and YZ directions. Two test prints were analyzed to determine the smallest resolvable features that could be obtained by the system. It was determined the minimum feature size obtained was 200 µm (XY) (with an error percentage of 5-8%), the minimum layer height obtained was 20 µm (with an error percentage of 1-2%), and the maximum build volume was 6 x 8 x 60 mm [9]. Lambert comments these tolerances were subjective based on the part geometry, resin formulation, and mechanical limitations of the instrument. The layer height tolerance was based off the ability of the stepper motor (which controls the build platform) to precisely move 20 µm after each layer was recoated, Lambert did not test the minimum layer height to be achieved with the PPDGA resin formulation, only as a function of the stepper motor used to move the build platform during part fabrication. Lambert noted for this system, the z accuracy was poor, reporting error percentages greater than 100% for YZ and XZ measurements. This was attributed to the tested PPDGA formulation contained no UV absorber and the depth of penetration was larger than the intended YZ and XZ features. Lambert did not measure YZ and XZ tolerances with the addition of UV blocker, as the goal of his work was to benchmark the

tolerances of the system, not the resin formulation. However, upon the addition of Tinuvin 400, a UV blocker, with increasing concentrations, Lambert reported the z-dimensional over cure was reduced from 500 µm to nearly 5 µm at the highest concentration of Tinuvin 400 (this corresponds to a reduction in 50% error to roughly 5% based off of Lambert's intended scaffold design). Lambert also reported at too high of UV blocker concentrations it was possible for layers to under cure, reducing the intended z-height of a printed scaffold.

Additionally, although the minimum feature size was reported to be 200 µm, in practice 200 µm size features may not be resolved. For this work, the intended pore sizes were 1 x 1 x 1 mm (1000 µm in each direction) and the layer height was set to 100 µm. This should require 10 layers to resolve a 1 mm feature size. Across 10 cured layers, unless the resin formulation has been optimized, the user may encounter under cure, over cure, and/or infill issues that would reduce the overall print fidelity from the intended structures. This could potentially result in a structure that has smaller or larger feature sizes based on resin formulation.

After taking the work of Lambert into account, and their validation of tolerance and % error for this particular µSL system, it was decided the % error from the .STL file would be assessed based off the % error in tolerances that Lambert discovered in order to assess print fidelity. Thus, for resolvable features such as pore height (YZ), pore width (XZ), pore length (XY), scaffold width (X), and scaffold height (Z), it was decided that < 10 % error would be deemed a "very good" print, 10-20 % error would be deemed an "good" print, and > 20 % error would be classified as a "poor" print. This was based off of the minimum feature size (XY) Lambert reported. Although Lambert reported z tolerances for this system were greater than 100%, this

was due to the high depth of penetration of PPGDA and lack of UV blocker in the resin formulation, so it is impractical to assess the z accuracy based off of reported z % error. The GelMA resins tested in this work do contain UV blocker (sulisobenzone) which will alter the overall z accuracy (as Lambert discovered with Tinuvin 400). Since Lambert found that the tolerances for layer height were much more accurate (since this is a mechanical limitation of the stepper motor), it was decided that for layer height measurements 1-5% error would be deemed "very good," 5-15% error would be "good," and anything greater than 15% error would be classified as "poor."

2.6 Cell Culture

All cell culture experiments were performed on 1 mm thick GelMA films in 24-well plates. The GelMA films were placed in PBS overnight, then washed 3 times with 70% ethanol, followed by 2 washes with PBS (1 hr each at 37 °C), and placed in media in the incubator (37 °C) overnight prior to seeding. The media was removed prior to cell seeding at 2 x 10^4 cells/well in 50 ~ 100 µL fresh media. The cells were allowed to adhere to films for 2 hr and fresh media added to a total working volume of 500 µL. Cells were allowed to proliferate for 1 to 3 days. At each time point, films (n = 3) were moved to a new 24-well plate and an MTS assay was used to quantify cell number via UV-Vis spectroscopy at 490 nm [58]. The cell density of films was reported using the obtained cell number divided by the surface area of the GelMA films (film diameter 14 mm). Qualitative analysis of the stained cells was used to gain insight into how the cells adhered to the GelMA films in terms of their morphology and density. One film from each resin was

stained for nuclei and cytoskeleton actin formation via DAPI and Texas Red stains respectively and visualized using a Zeiss Confocal Microscope.

2.7 Statistical Analysis

All experiments where run in triplicate (n = 3) including the 3D printed structures and image analysis. Microsoft Excel was used to run one-way single factor ANOVA tests. If the test revealed that $F > F_{critical}$ then it was determined that one or multiple samples do not belong to the same population, thus there could be significance between groups. The Bonferroni approach was then used with a post hoc test to further analyze groups. This approach included two sample t-tests assuming equal variances that were run to compare within and between groups. Significance was determined if $p < 0.05$. Not all experiments required statistical analysis. Results are reported with significance markers as well as the average ± standard deviation.

Chapter 3: Results and Discussion

3.1 NMR Confirmation of Gelatin Modification

^{1}H NMR utilizes an external magnetic field to aid in the determination of the structure of a molecule and was used to confirm gelatin modification. The resulting spectra of gelatin and GelMA were compared and integrated to determine the degree of methacrylation (the estimation of substitution, DS, of methacrylate groups per amine group on the gelatin backbone). For plain gelatin (Figure 3-1A), the peaks at a and b correspond to the lysine methylene and methyl functions respectively, that will change upon methacrylation. New peaks appear at 5.6 ppm and 5.4 ppm (c and d respectively, Figure 3-1B) which correspond to methacrylic functions from the acrylic protons. Additionally, peak b increases in intensity, corresponding to a methyl group; while peak a decreases in intensity. This disappearance corresponds to a reduction in the lysine methylene peak from plain gelatin at 2.9 ppm; suggesting lysine residues were reacted. Each of the relevant peaks discussed were present in all of the spectra collected during experimentation, and a total of 10 syntheses were performed to produce modified gelatin (GelMA) for this work. The average batch size was approximately 10 g per batch, with a yield of 90% or more of GelMA.

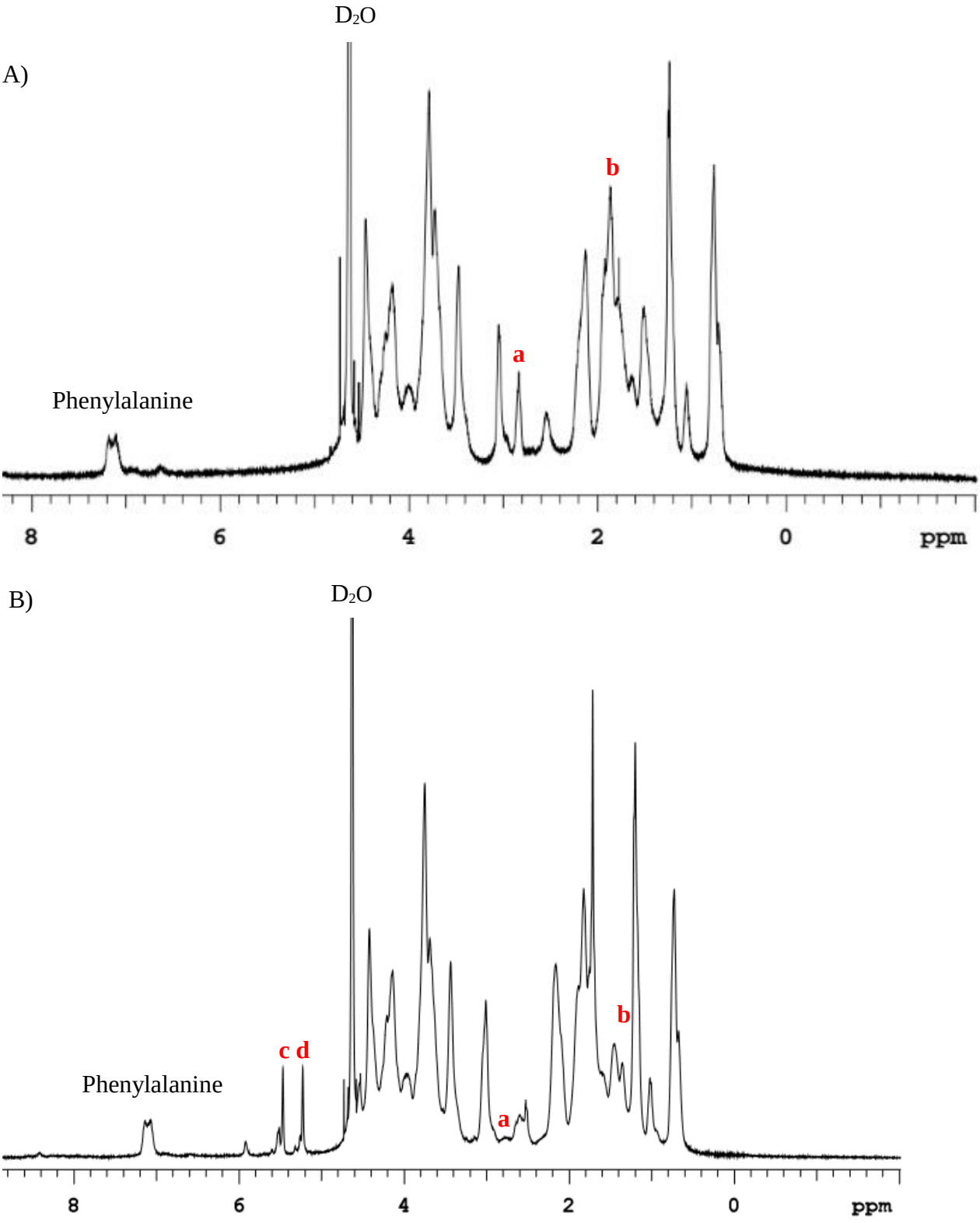

Figure 3-1: Representative ^{1}H NMR of A) Type B Gelatin as received and B) GelMA after modification. The phenylalanine peak was used to normalize the spectra. Peaks a (2.9 ppm) corresponds to lysine methylene signal and b (1.9 ppm) corresponds to the methyl signal. Peaks c and d were observed at 5.6 and 5.4 ppm and correspond to methacrylic functions from acrylic protons.

To determine the DS of GelMA, the two spectra from Figure 3-1 were first normalized using the phenylalanine peak as reference. The area under 2.9 ppm was compared between the two spectra using Equation 2-1 to determine the DS. The DS was found to be 54% +/- 4% across 10 syntheses and was considered to be a medium level of substitution. According to the literature high DS is considered to be above 80%, while medium is around 50% and low is around 20% [24, 35]. Some researchers have focused on the DS in order to optimize the total modification of gelatin [24]. GelMA syntheses up to 95% DS have been reported [24]. However, for the purposes of this research, the focus was not on the synthesis of GelMA. The goal here was to modify gelatin in order to achieve enough methacrylate groups so a photoactive resin would be created – this was achieved. Investigating the impact of DS on the resulting GelMA resins could be future work. A higher DS corresponds to more methacrylate groups per volume. This in turn would increase the reactivity of the resulting GelMA resin. A higher DS resin would also likely have a higher molecular weight, which would contribute to an increase in viscosity of GelMA resin [24, 25, 34, 48]. If the resin is too viscous the build stage would not be able to move and curing consecutive layers would become difficult. Additionally, a higher DS may alter the gel point of the resin. For µSL it is optimal to have a resin that prints at room temperature, so heating and stirring are not necessary to maintain a homogenous solution or lower the solution viscosity. Again, it was determined for the purposes of this research, 50% DS was suitable to produce 3D printed constructs. However, the low concentration GelMA resins (L-GelMA 1 and L-GelMA 2) did not create suitable printing resins. This could be a result of the DS. Achieving a higher DS (around ~80%) may mean printing lower concentrations of GelMA (~10 w/w %) could be achievable due to a higher volume of methacrylate groups.

3.2 Photo-Rheology

Photo-rheology employs a similar methodology as rheology, but with a UV curing attachment. In rheology, oscillatory measurements are taken over a time or temperature range in order to gain insight on the rheological properties of a material. Rheological properties refer to the storage modulus (G') and loss modulus (G'') of a material that translate to a materials behavior as solid or liquid respectively. If the storage modulus dominates then the material is deemed solid-like, if the loss modulus dominates then the material is deemed liquid-like. With rheology, the G' often corresponds to the overall stiffness of a material, the higher the G', the more stiff or mechanically robust a material is. Photo-rheology in particular is a useful tool to determine not only viscoelastic properties of a material, but also its relative printability/chemical reactivity in the presence of a UV light source. Photo-rheology was thus employed as a probing technique to observe potential printability parameters of GelMA such as cure time and layer thickness.

A)

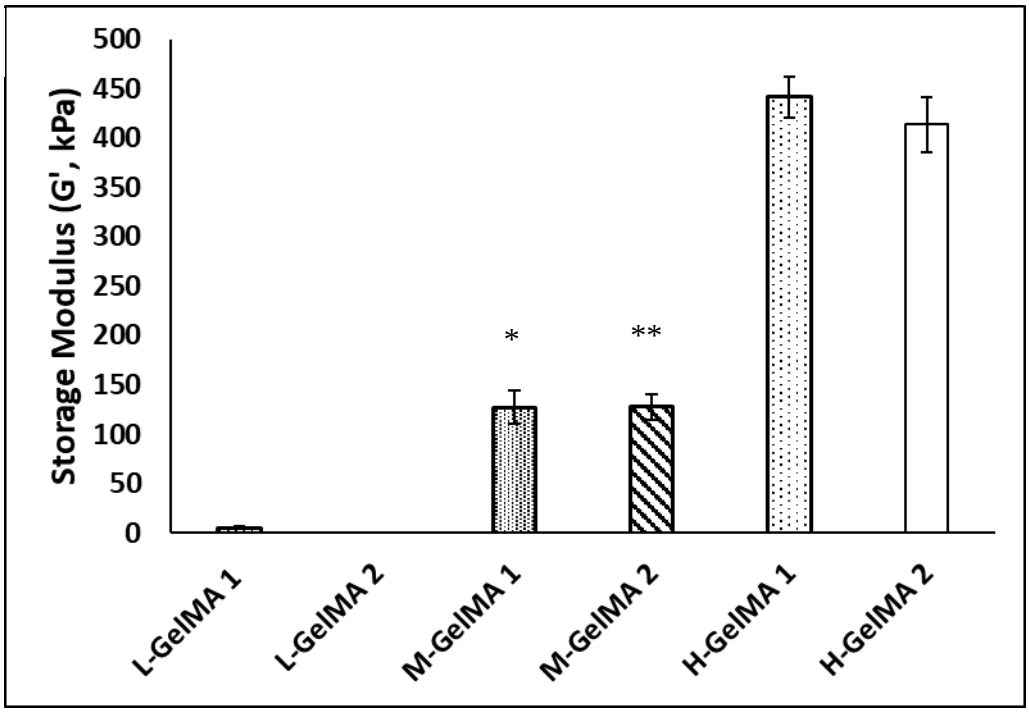

B)

	Gel Point (sec)
L-GelMA 1	4.7 ± 0.11
L-GelMA 2	N/A
M-GelMA 1	3.1 ± 0.77***
M-GelMA 2	4.0 ± 0.25**
H-GelMA 1	1.9 ± 0.11*
H-GelMA 2	2.9 ± 0.28*

Figure 3-2: A) Photo-rheology data of GelMA samples (w/w %) (refer to Table 2-1 for exact concentrations). M-GelMA 1 was significantly different than H-GelMA 1 and H-GelMA 2 (*$p < 0.001$) and M-GelMA 2 was significantly different than H-GelMA 1 and H-GelMA 2 (**$p < 0.001$). Both M-GelMA and H-GelMA resins were significantly different than L-GelMA resins ($p < 0.001$), while L-GelMA 1 was significantly different than L-GelMA 2 (where no data could be collected, this same trend applies to 3-2B)). B) The gel point was determined as the crossover point between G' and G'' and was reported across all samples. H-GelMA 1 was significantly different than H-GelMA 2 (*$p < 0.05$), while M-GelMA 2 was significantly different than H-GelMA 1 and H-GelMA 2 (**$p < 0.005$), and M-GelMA 1 was significantly different than H-GelMA 1 (***$p < 0.05$). Experiments were run in triplicate ($n = 3$) and reported as the average ± standard deviation.

Figure 3-2A demonstrates with increasing GelMA concentration, the storage modulus (G') of the GelMA significantly increased ($p < 0.001$). This phenomenon is well described in the literature [9, 18, 29, 50]. It was difficult to comparison the storage modulus among the literature, because most research on GelMA quantifies mechanical properties of resins formed from 5, 10, and 15 w/w% respectively, without the addition of UV blocker and instead utilizing Irgacure 2959 as a photoinitiator [18, 27]. Thus, the mechanical properties reported in this research are unique to this particular system/formulations of GelMA resins. However, the trend in the mechanical properties corresponds to that reported in prior literature. Nichol *et al* 2010 reports regardless of altering the DS, at 10% and 15% (w/w) concentrations of GelMA, the compressive modulus of their GelMA films increased with increased concentration of GelMA [35]. They also found at consistent DS the compressive modulus of their films increased with increasing GelMA concentration [35]. This indicated at certain concentrations of GelMA, the DS may not impact

the mechanical properties, but the concentration will. Looking at rheological properties, Van Den Bulcke *et al* 2000 investigated both the effects of gelatin and GelMA without photoinitiator and with UV curing [36]. Their research showed at temperatures greater than 40 °C the physical properties of gelatin and GelMA change as the physical network of gelatin "loosens" upon reaching its melting point. However, as concentrations of GelMA increased from 10% w/v to 20% w/v the storage modulus of cured films of GelMA increased as well [36]. Van Den Bulcke *et al* 2000 also reported an average storage modulus of approximately 10 kPA for GelMA films produced at 15 w/v % and 40% DS [36]. In comparison to the results shown in Figure 3-2A, the GelMA produced in this research is a 10 fold increase in the storage modulus and a trifold increase upon that of 30 w/w % GelMA. This current work suggests the increase in storage modulus for GelMA is exponential depending on the concentration. However, the synthesis performed in this work was different than that used in Van Den Bulcke *et al* 2000 and previous reported literature. The concentrations and DS explored in this research were higher than those explored in Van Den Bulcke *et al* 2000. The trends observed from this work are consistent with those across past literature, even though the material system and concentrations are novel.

As shown in Figure 3-2B, as GelMA concentration was increased, the gel point (time at which the storage modulus supersedes the loss modulus) decreased ($p < 0.05$). This was attributed to a higher concentration of photo-active (methacrylate) groups present within the higher concentrations of GelMA. Also, when the UV blocker concentration was increased the gel point increased for the H-GelMA formulations (Figure 3-2B). The UV blocker absorbs UV energy and thus prevented the system from curing as fast, in turn raising the gel point. However, for M-GelMA 1 and M-GelMA 2 resins only the GelMA concentration had an impact on the overall

cure time, not the concentration of UV blocker. This is suggested by the M-GelMA 2gel point being significantly higher ($^{**}p < 0.005$) than both H-GelMA 1 and H-GelMA 2. However, M-GelMA 1 was only significantly higher ($^{***}p < 0.05$) than H-GelMA 1, meaning that at a lower concentration of GelMA and UV blocker, this resin may behave similarly to H-GelMA 2 in terms of its gel point and potentially its printability parameters. This may indicate more UV blocker would be required for this specific concentration to yield a significant effect on the printability of M-GelMA resins.

Photo-rheology was also useful in gaining insight into the printability of the GelMA resins. Since the gap height in the photo-rheometer is set to 0.5 mm, uniform 0.5 mm films cure, and when the storage modulus reaches a constant value this was determined to be the full cure of the system. Figure 3-3 shows this full cure occurred within 90 s for all GelMA concentrations. This gave insight toward the overall print time and layer thickness to be expected from GelMA when used in µSL. Since one of the primary goals was to produce layers less than 200 µm faster than currently researched GelMA resins, the photo-rheology data gives preliminary data for what parameters to set in the LabView program prior to printing. A cure time of 90 s per layer would be far too high for reaching the desired print fidelity. This was a good indication of an improvement on current µSL GelMA resins, because typical cure times are on the magnitude of 5 ~ 30 min for a print. This would correspond to 32 s exposure per layer based off of the intended structure (see section 3.6). For this work, the highest cure time per layer was 1.6 s (section 3.6) which is a massive improvement given the current state of the art.

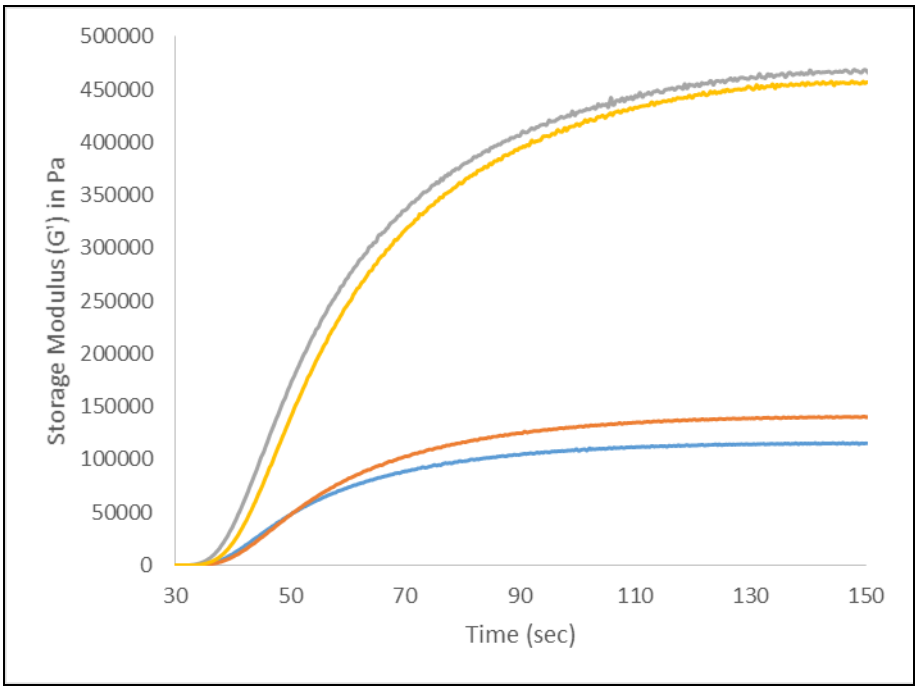

Figure 3-3: Photo-rheology data of the average G' of GelMA samples (w/w %). From bottom to top, the lines represent M-GelMA 1 (blue), M-GelMA 2 (orange), H-GelMA 1(yellow), and H-GelMA 2 (gray). The L-GelMA data was not included because these two formulations were deemed unsuitable for further study. All experiments were run in triplicate (n = 3).

3.3 Photo-DSC

Like Photo- rheology, photo-DSC also utilizes the same principles of DSC, but with a UV curing attachment. The photo-DSC gives insight into the curing reaction of photo active resins by measuring the heat flow or energy required to fully cure a system over time. Since GelMA is derived from a natural polymer, it is inherently less photoactive than synthetic materials such as PEGDA and contains less photoactive groups. GelMA forms a hydrogel material, meaning > 80% of the structure is water, with synthetic resins this is the complete opposite, where > 80% of the structure is monomer that can be cured, making synthetic resins much more photoactive. Much like with photo-rheology, photo-DSC was used as a probing technique to gain insight toward printability and functionality of GelMA resins. Figure 3-4A represents the heat flow as a

function of time for respective GelMA resins. L-GelMA resins were not included because their heat flow was too low to display on the graph and they were deemed unsuitable for further testing. The heat flow is negative, indicating an exothermic reaction and crosslinking. A negative heat flow is common for these types of reactions as the resin has a lower heat flow than that of the reference pan. The specific heat in Figure 3-4B is determined by integrating the area under the heat flow graph in Figure 3-4A.

A)

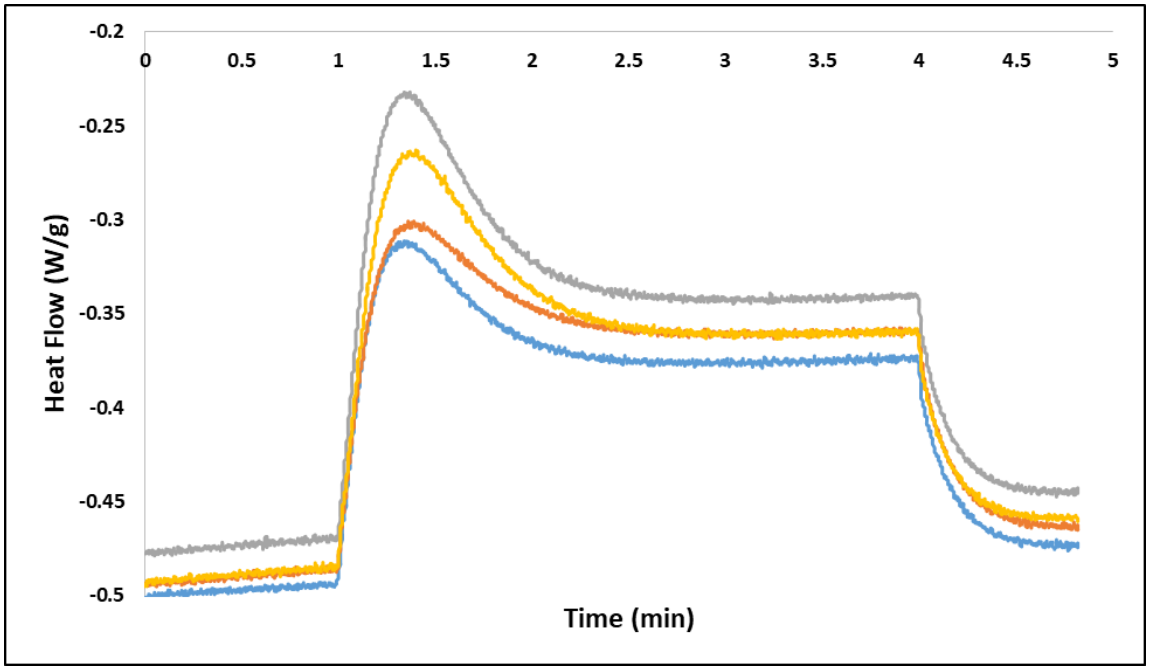

B)

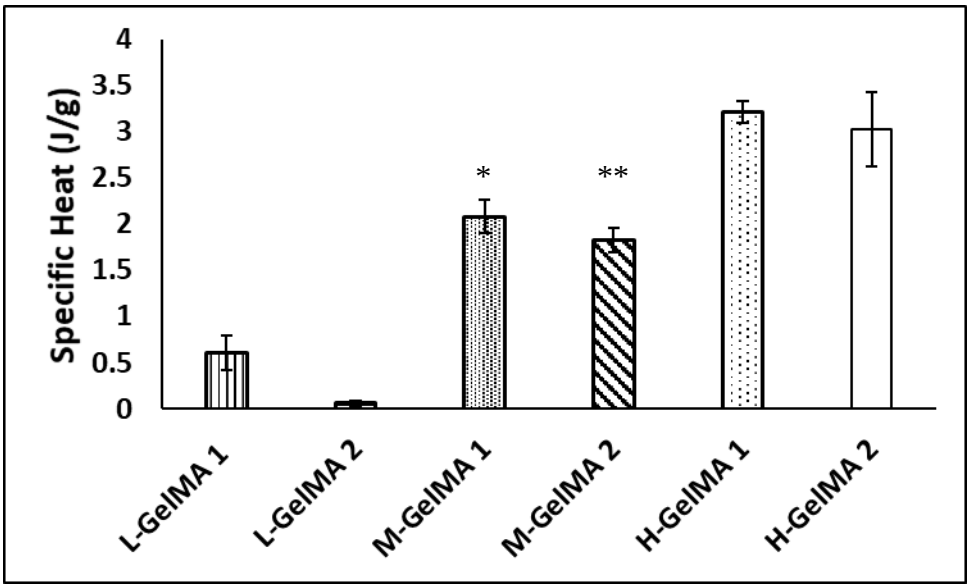

C)

	Cure Time (sec)
L-GelMA 1	38 ± 1.4
L-GelMA 2	50 ± 0.0
M-GelMA 1	33 ± 1.1***
M-GelMA 2	42 ± 4.2**
H-GelMA 1	34 ± 2.5*
H-GelMA 2	43 ± 4.3*

Figure 3-4: A) Representative Photo-DSC curves of GelMA samples (w/w %). From bottom to top, the lines represent M-GelMA 1 (blue), M-GelMA 2 (orange), H-GelMA 1 (yellow), and H-GelMA 2 (gray). The low concentration GelMA samples were not included on the graph because their heat flow was too low to display properly and they were deemed unsuitable compositions. B) Calculated average specific heat of GelMA samples (w/w %). M-GelMA 1 was found to be significantly different than H-GelMA 1 and H-GelMA 2 ($^{*}p < 0.05$) just as M-GelMA 2 was found to be significantly different than H-GelMA 1 and H-GelMA 2 ($^{**}p < 0.005$). C) Average cure time based upon the time at which the highest peak occurs. H-GelMA 1 was significantly different than H-GelMA 2 ($^{*}p < 0.05$), while M-GelMA 2 was significantly different than H-GelMA 1 and M-GelMA 1 ($^{**}p < 0.05$), and M-GelMA 1 was significantly different than H-GelMA 2 and M-GelMA 1 ($^{***}p < 0.05$). Refer to Table 2-1 for exact concentrations. Experiments were run in triplicate (n = 3) and reported as the average ± standard deviation.

Originally three GelMA concentrations were to be tested (see Table 2-1), but almost immediately the 10% GelMA concentration was eliminated because it was unable to cure properly as observed in both photo-rheology and photo-DSC. The 10% solutions were turbid upon production, which was the first indication of their potential failure. The turbidity was attributed to insolubility between GelMA and sulisobenzone, an indication from particulates that were present in 10% solutions. First, from photo-rheology the lack of a gel point for L-GelMA 2 was a strong indication that this formulation would fail. Photo-DSC then further supported the elimination of the 10% GelMA concentration from the printable resins. Therefore, it was deemed L-GelMA 1 and L-GelMA 2 would be inadequate to explore for 3D printing, so from this point on the other four resins from Table 2-1 were explored. Similar to photo-rheology, photo-DSC observed increasing GelMA concentration significantly increased the energy (specific heat, J/g)

absorbed by the system. This was expected since higher concentrations of GelMA have a greater concentration of monomer available to react and initiate free radical polymerization.

Unlike photo-rheology which gives a rough estimate of the initial cure time based on the gel-point and the total cure time based on the storage modulus, photo-DSC yields an absolute measurement of the total time required to completely cure the resin as it measures the total energy required to cure. This is useful not only for post-curing procedures of 3D printed scaffolds, but it also gives insight into the total printing time of the resin system, or the total energy and time required to react the monomers completely. The highest reported time (Figure 3-4C) was 50 s and agreed with the 90 s total cure time found in photo-rheology. This overall cure time suggests larger 3D printed structures of GelMA could be produced in a fraction of the time compared to extrusion-based methods.

Statistical analysis described in Figure 3-4C further suggested the overall cure time of the resin is impacted by both the GelMA concentration and UV blocker. As seen with H-GelMA 1 and H-GelMA 2, with increasing UV blocker concentration, the cure time increased for similar GelMA concentrations ($p < 0.05$). This is because the UV blocker absorbs some of the UV energy preventing it from interacting with the GelMA and LAP. There is an obvious formulation interplay that occurred between M-GelMA and H-GelMA resins. Since the photoinitiator was held constant, the two factors that affected the characterization were UV blocker and GelMA concentration. At different GelMA concentrations but same UV blocker concentrations there was no significant difference in cure times. However, at higher concentrations of UV blocker the cure time was significantly affected. Although the UV blocker concentration had no impact on the

rheological properties of the formulations, it is definitely apparent that the UV blocker concentration had an impact on the kinetics of the reaction and overall cure times of each formulation tested.

3.4 Swell Testing

Having officially ruled out the L-GelMA resins from any further characterization, the next step was to test the overall water content of hydrogels formed with the remaining formulations. Swell testing is a common method for hydrogel materials to determine the overall water capacity within the physical network of the material. In the literature, it is a common trend that increasing GelMA concentration decreases the overall water content of subsequent hydrogels [25, 33, 35, 36, 42, 53, 55]. The swollen weight of a hydrogel can affect cell nutrient diffusion and transport, as well as the mechanical properties of the hydrogel. Thus, the higher the water content in a material, the less mechanically robust it may be, but it may be more efficient at transporting waste and nutrients to mimic a cellular microenvironment. Table 3-1 depicts the results from swell testing with M-GelMA and H-GelMA resins. Significantly higher swelling ($p < 0.05$) was experienced by lower concentrations of GelMA, while less swelling was observed for higher concentrations of GelMA, which agreed with previous reports [25, 33, 35, 36, 42, 53, 55]. Higher concentrations of UV blocker resulted in less swelling ($p < 0.05$), while lower concentrations of UV blocker resulted in greater swelling. A higher UV blocker concentration correlated to a lower swell percentage, which could in turn result in reduced cell proliferation and viability. Swelling properties also have the potential to effect mechanical properties. Photo-rheology data did not detect a significant impact on the storage modulus of GelMA films for M-GelMA and H-GelMA resins with different UV blocker concentrations (but, these films were not

swollen when rheological tests were run). The swelling was less for M-GelMA 2, and H-GelMA 2, and both these compositions have higher UV blocker concentrations. The polymeric networks of these resins could be more crosslinked than their lower UV blocker concentration counterparts. This could be due to the fact there would be additionally energy required (as shown in the photo-DSC data) to cure resins with higher UV blocker concentrations. This energy could correlate to higher crosslinking within the hydrogels, preventing the same amount of swelling between formulations from occurring. It is also key to mention that these resins swell considerably, and this may have an impact on overall print fidelity. During the printing process the 3D printed part is lowered back into the resin vat after each layer. There may be residual swelling that occurs during this process as well as post-washing of the scaffolds that swells the 3D printed part and impacts the overall print fidelity (this could result in a reduced feature size such as pores, contributing to the deviation from the .STL file/intended 3D print structure).

Table 3-1: Average swell percentage of GelMA resins. Significance was found between M-GelMA 1 and M-GelMA 2 ($^{**}p < 0.005$) as well as H-GelMA 1 and H-GelMA 2 ($^{*}p < 0.05$). All experiments were run in triplicate (n = 3).

	% Swelling
M-GelMA 1	$426 \pm 2^{**}$
M-GelMA 2	$344 \pm 6^{**}$
H-GelMA 1	$284 \pm 1^{*}$
H-GelMA 2	$240 \pm 4^{*}$

3.5 Working Curve

As discussed in section 2.5.1, the working curve is a crucial component of developing any resin for 3D printing with SLA. The working curve relates the exposure of light delivered at the prepolymer surface (E) to the depth at which the prepolymer is crosslinked, also known as the cure depth (C_d). The minimum exposure required to begin polymer crosslinking is the critical

exposure (E_c). The working curve gives insight to the amount of UV energy and time required for photopolymer curing. Figure 3-6 revealed H-GelMA 1 has the lowest critical exposure, which was expected since H-GelMA 1 has the highest GelMA concentration and lowest UV blocker concentration. M-GelMA 2 has the longest critical exposure, but lowest depth of penetration. This was also expected as M-GelMA 2 has a lower GelMA concentration and highest UV blocker concentration. Increasing GelMA concentration would decrease exposure time because there is a higher amount of methacrylate groups per volume of the pre-polymer (Table 3-2). However, increasing UV blocker concentration would increase exposure time because more free radicals will be scavenged by the UV blocker instead of the monomer. Based off of Figure 3-6, the most promising resin prior to 3D printing would be M-GelMA 2, because the layer thickness and depth of penetration are lowest, meaning theoretically this resin should produce the smallest layers in a 3D printed scaffold. The only drawback would be it has a higher critical exposure, which could mean a 3D printed scaffold from M-GelMA 2 would take longer to print compared to H-GelMA 1, but it would be more difficult to introduce porosity into a resin from H-GelMA 1 because it has a larger depth of penetration. A larger depth of penetration means that if the targeted layer height for printing is 100 µm, and the depth of penetration of the resin is > 100 µm, consecutive layers would experience UV exposure past the layer height (over cure). If UV exposure is bleeding into consecutive layers then over curing will occur and fill any negative space or porosity that was intended for the scaffold. However, this appeared to only be the case for the H-GelMA 1 resin. The result of the working curve was promising for producing the intended GelMA scaffold with a layer height of 100 µm and choosing µSL as a method over extrusion for this type of resolution.

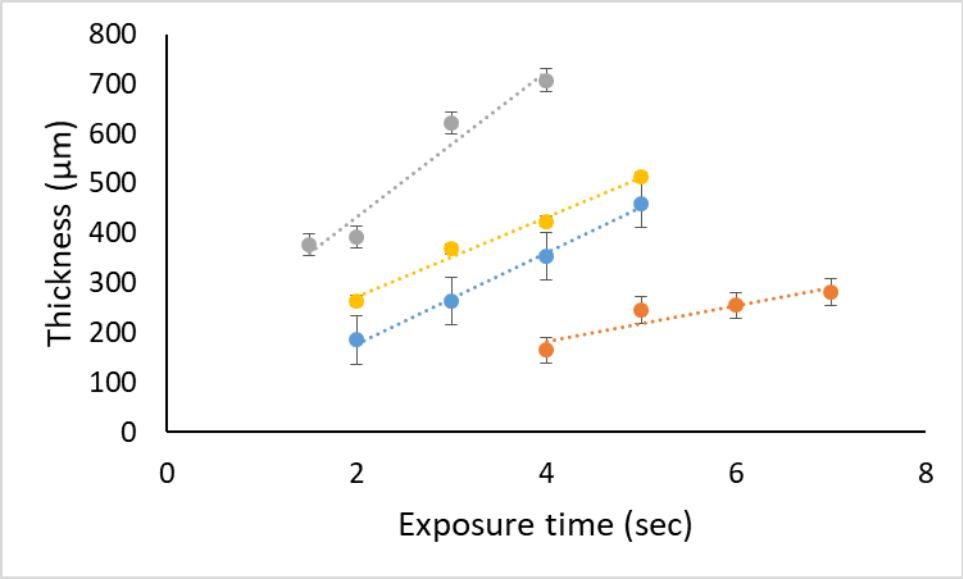

Figure 3-5: Working curve of GelMA Resins H-GelMA 1 (gray), H-GelMA 2 (yellow), M-GelMA 1 (blue), M-GelMA 2 (orange). Measurements were taken in triplicate (n = 3) and the error bars represent the average standard deviation.

Table 3-2: From Figure 3-6 the following values were derived. The D_p corresponds to the slope of the trend lines while the E_c corresponds to the x-intercept.

	Depth of penetration (D_p) (µm)	**Critical exposure (E_c) (s)**
M-GelMA 1	91.60	0.06
M-GelMA 2	35.94	1.08
H-GelMA 1	145.62	0.98
H-GelMA 2	80.38	1.38

3.6 3D Printing Analysis

3D print images were divided into five different categories: scaffold face measurements, top of scaffold measurements, bulk scaffold measurements, pore measurements, and scaffold layer measurements. The analysis was based off of the .STL file in Figure 2-1 of a 4 x 4 x 5 mm (l, w, h) rectangular 3D scaffold. Figure 3-7A and 3-7B show representative images of a scaffold with the measurements labelled for both the face and the top of a scaffold respectively. Figure 3-7C depicts the printing parameters that were informed from the previous

characterization techniques: photo-rheology, photo-DSC, and working curve in order to reach the minimum exposure time require to generate a 3D structure. The layer height was kept constant to reduce the variables and measure how precise the limit could be met with various resins.

A)

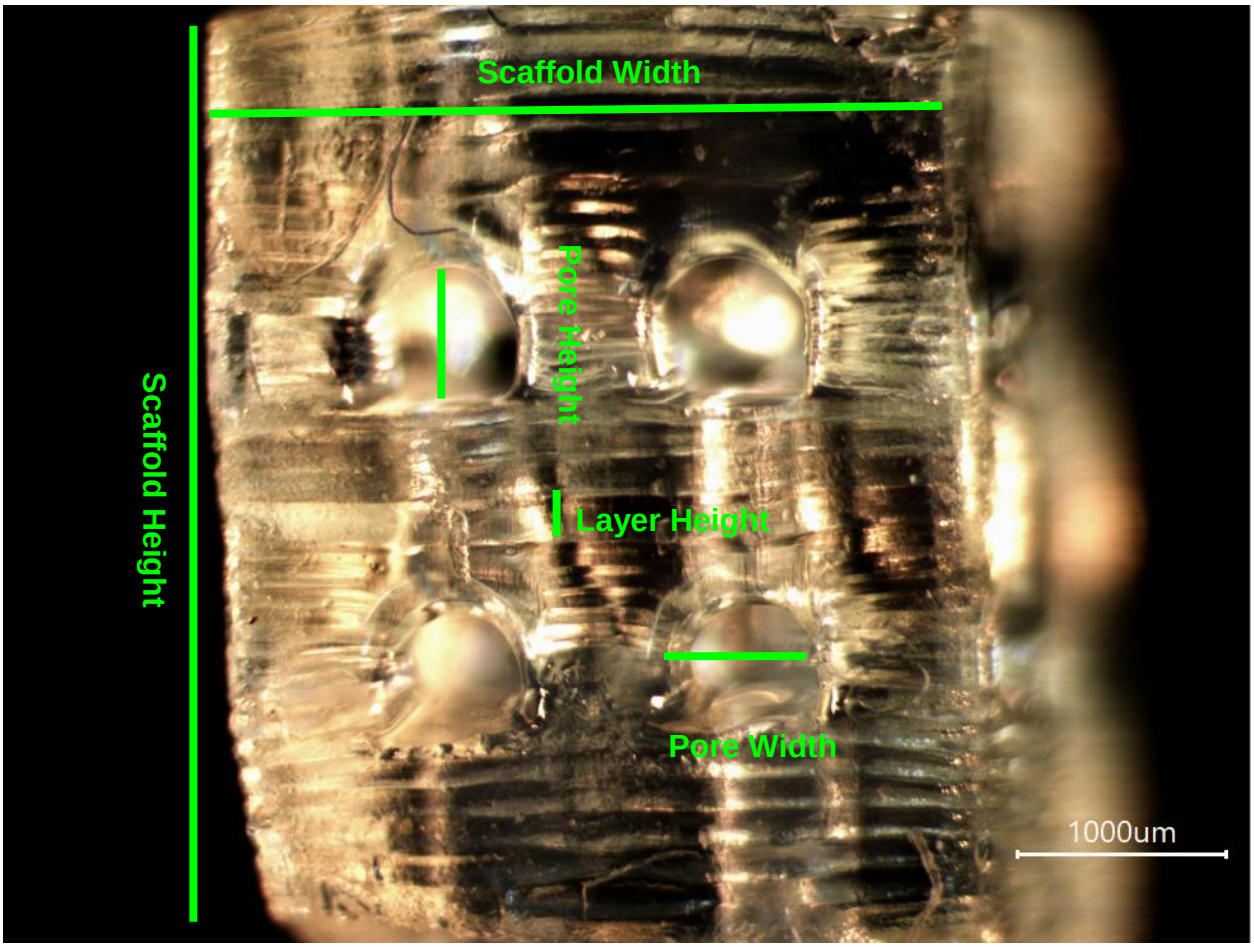

B)

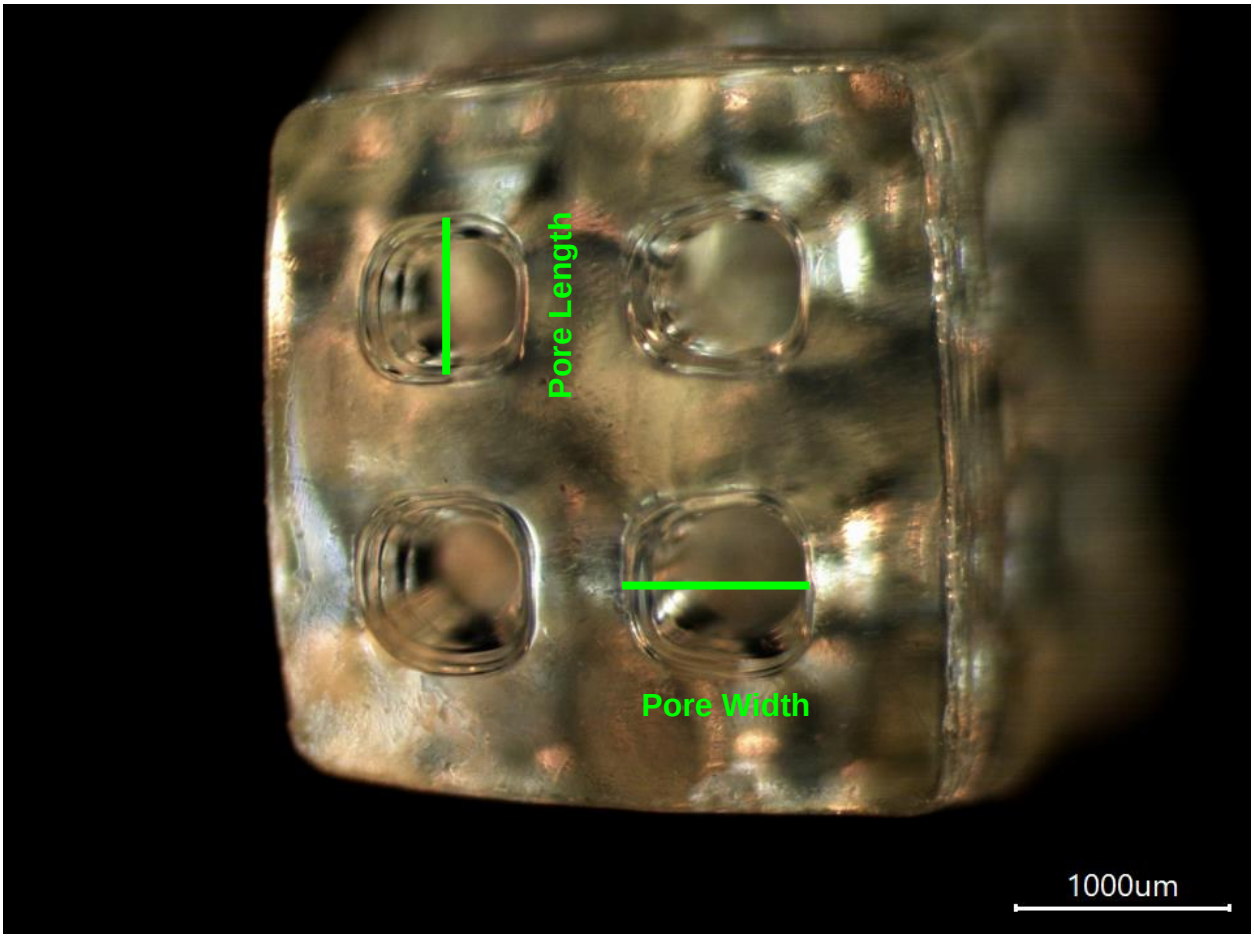

C)

	Layer height (μm)	Exposure time (ms)
M-GelMA 1	100	900
M-GelMA 2	100	1600
H-GelMA 1	100	700
H-GelMA 2	100	1200

Figure 3-6: Representative light images of GelMA scaffolds with features measured of the A) scaffold face and B) scaffold top. C) Table depicting printing parameters input into the LabView software for each resin type, the pore size for each scaffold type was 1 mm in diameter.

A face of scaffold (Figure 3-7A) measurement was deemed to be one of the four sides of the cube. Multiple faces were measured per scaffold to obtain a total of 10 measurements per parameter. A top of scaffold (Figure 3-7B) measurement came from the last layer printed (top face, one per scaffold). A bulk scaffold measurement was deemed to be a bulk dimension of the scaffold such as total length or total width across the cube (Figure 3-7A). The pore width was

defined as the total distance across the pore in the x-direction. The pore height was defined as the total distance across the pore in the z-direction. The pore length was defined as the total distance across the pore in the y-direction. A layer measurement was defined the height of the layer generated from the 2D projection exposed on the resin surface, and was averaged over several layers. Refer to Chapter 2: Materials and Methods for how the images were taken and how many measurements were taken per scaffold.

3.6.1 Scaffold Face Measurements

For the scaffold face measurements, pore height and pore width were analyzed. Pore height in each scaffold was intended to be 1 mm across. Pore height was considered significant in that it composes the z-direction of the pore and helps produce the negative feature. Ideally, each pore would be perfectly square, but that was not the case for the GelMA prints here. In Figure 3-8 the only significant difference reported for the pore height was with H-GelMA 2 ($p < 0.05$). H-GelMA 2 had a larger pore height than the other formulations. This suggested at a high concentration of GelMA and UV blocker, a significant impact on the pore height fidelity was made. The trend observed in Figure 3-8A show an increase in pore height across resins, while the trend overserved in Figure 3-8B show a decrease in % error. H-GelMA 2 was not only significantly larger ($p < 0.05$) in terms of its pore height than all other resins, but also had the lowest % error which was the first indication H-GelMA 2 could be a good resin formulation for GelMA printing with µSLA.

A)

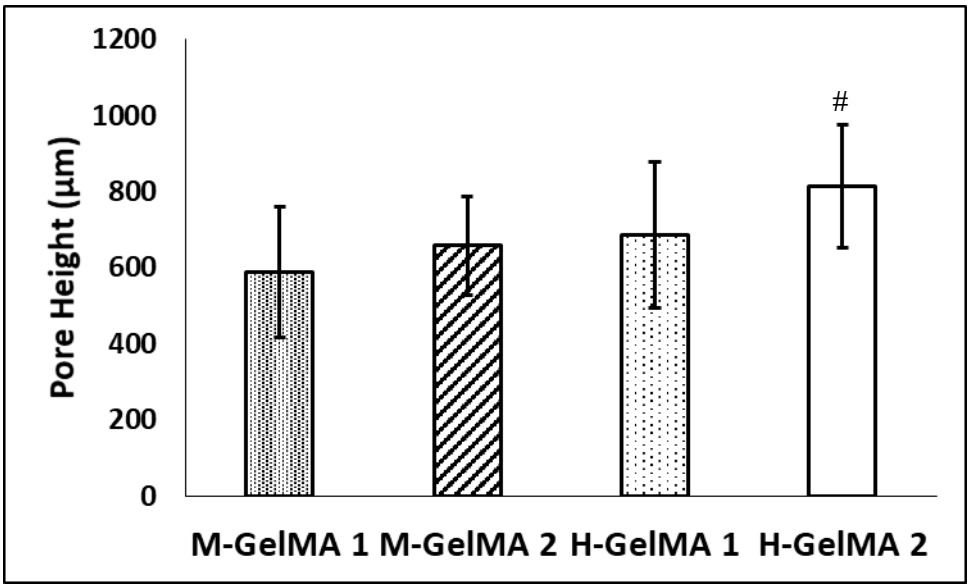

B)

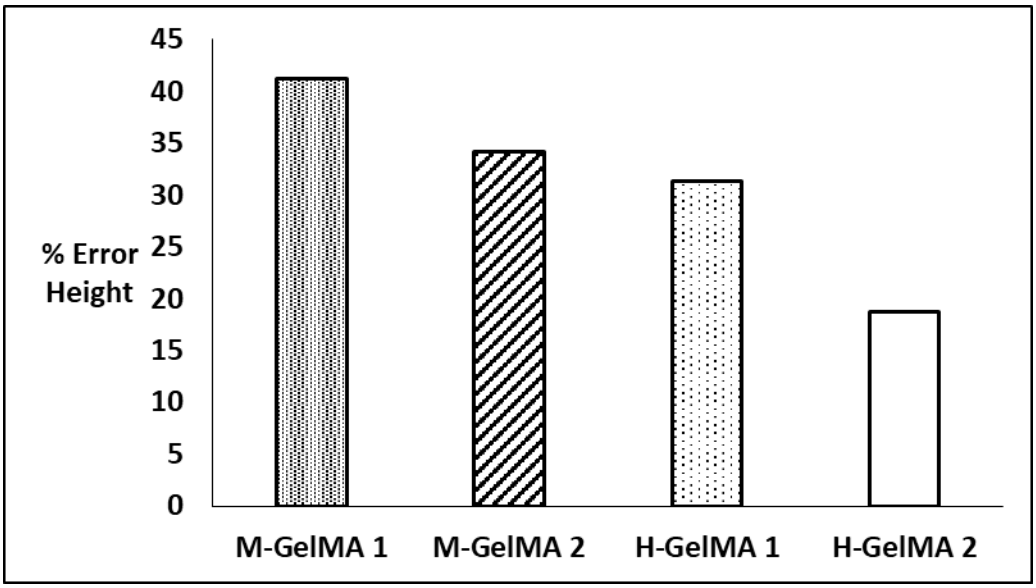

Figure 3-7: A) Pore height measurements and standard deviations for faces of printed GelMA scaffolds (n = 10). For the pore height, only H-GelMA 2 was significantly different ($^{\#}p < 0.05$) than all other GelMA resins in terms of the pore height measurements. B) Percent error bar graph depicting the deviation between GelMA Resins and the theoretical pore height measurements.

Next, the pore width measurements were analyzed. Pore width in each scaffold was intended to be 1 mm across. Pore width was considered significant in it composes the x-direction of the pore and produces the negative feature with the z-direction of the pore. From Figure 3-9A it was apparent there was significant differences between the pore width measurements for all GelMA

resin types. More specifically, M-GelMA 1 and H-GelMA 2 resins were significantly different ($p < 0.001$) from all other resin types. M-GelMA 1 reported significantly smaller pore widths, while H-GelMA 2 reported significantly larger pore widths. This demonstrates how the resin formulation changes the overall fidelity of the final printed part. The lowest concentration of GelMA/UV blocker observed more over cure while the highest concentration of GelMA/UV blocker observed less over cure. This yields proof the GelMA concentration and UV blocker concentration have a direct impact on the fidelity of this scaffold type in terms of pore width. Since the intended pore width was 1000 µm, a comparison between the theoretical pore width and actual pore width was determined as the % error (Figure 3-9B). From this, it was determined that M-GelMA 1 had the largest deviation from the intended structure, while H-GelMA 2 again had the lowest deviation, which directly correlates to the observation in Figure 3-9A. Overall Figure 3-9 revealed the H-GelMA 2 resin had the highest print fidelity in terms of pore width on the scaffold faces across all samples.

A)

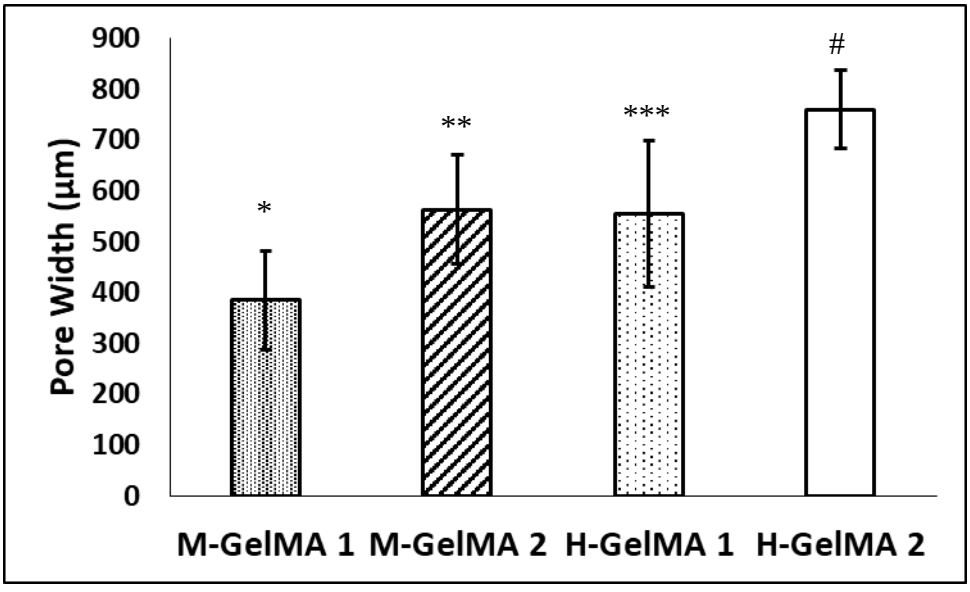

B)

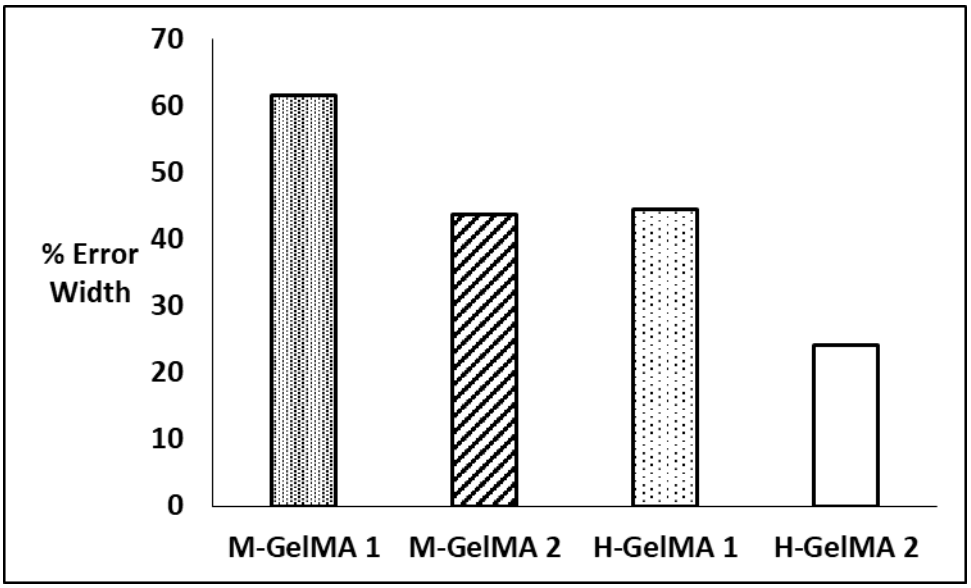

Figure 3-8: A) Pore width measurements and standard deviations for faces of GelMA scaffolds and resins (n = 10). M-GelMA 1 is significantly different than all other resins ($^{*}p < 0.001$). M-GelMA 2 is significantly different than M-GelMA 1 and H-GelMA 2 ($^{**}p < 0.001$). H-GelMA 1 is significantly different than M-GelMA 1 and H-GelMA 2 ($^{***}p < 0.01$). Lastly, compared to all other groups H-GelMA 2 is significantly different ($^{\#}p < 0.001$) than all other GelMA resins in terms of the pore width measurements. B) Percent error bar graph depicting the deviation between GelMA Resins and the theoretical pore width measurements.

Based off of these two categories, it was apparent there was more variation present in the pore width compared to the pore height. However, H-GelMA 2 stands out in both categories with the lowest percentage of error in each category (Figures 3-8B and 3-9B). In terms of printability of this resin system, it means 30% GelMA and 1.0% UV blocker yielded the best printability for these GelMA resins, but it still must be determined whether or not this H-GelMA 2 was successful in terms of the instrument specifications. H-GelMA 2 prints resulted in pores that were approximately 800 x 800 µm. This correlates to an error of roughly 20% in terms of both pore height and pore width. This was the lowest % error reported, and based off of the ranking system described in section 2.5.2 this was deemed a "good" print, while the other resin formulations all fell within the "poor" print category.

3.6.2 Top of Scaffold Measurements

Similar to the face scaffold measurements, the top of scaffold measurements were taken in reference to Figure 3-7B. The pore width and pore length bear the same significance as the pore width and pore height on the face of the scaffold. The top of scaffold is relevant because that is where the least amount of UV exposure is endured by the scaffold. As mentioned in section 3.5 regarding the working curve, depending on the depth of penetration and critical exposure, the scaffold can experience over curing due to the bleeding of excess UV light into consecutive layers of the 3D scaffold. The top of scaffold pore width and pore length are relevant to the overall fidelity of the 3D printed scaffold.

In terms of the pore length, M-GelMA 1 was significantly smaller than all other resin types (Figure 3-10A, $p < 0.001$) and has the highest % error of all other resin types (Figure 3-10B). This suggested M-GelMA 1 was not an ideal resin type for µSLA printing in terms of the pore length at the top of the scaffold. This was interesting as the top most layer of the scaffold experiences the least amount of UV exposure (due to the bottom-up manufacturing approach), one would expect the top layer to not have any significant differences across all resin types. This was another clear indication that GelMA concentration and UV blocker concentration indeed have a direct impact on the printability of the scaffold. In terms of printability, the % error in pore length for M-GelMA 2, H-GelMA 1, and H-GelMA 2 all fell between 10-20%, meaning these prints were “good” in terms of pore length. M-GelMA 1 was above 20% error and deemed a “poor” print.

A)

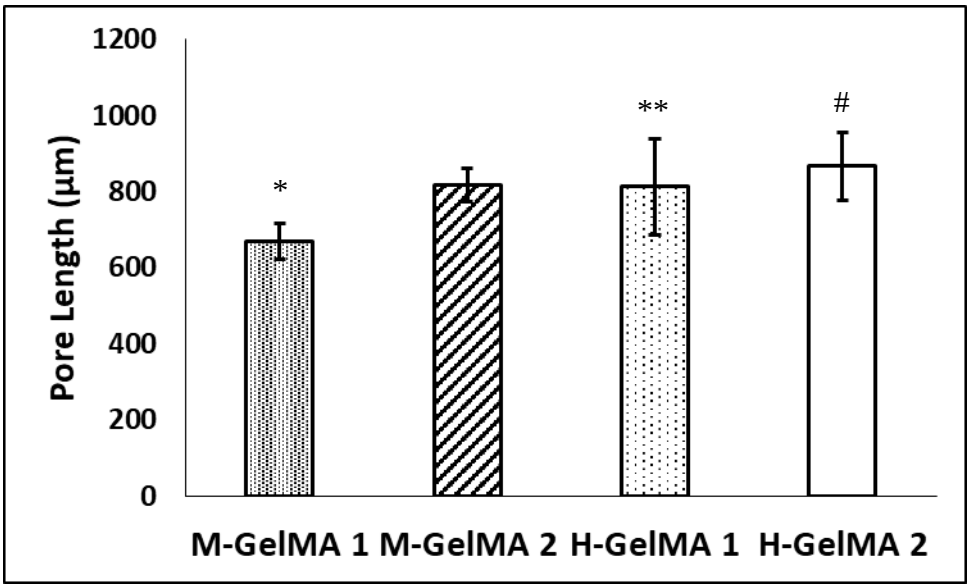

B)

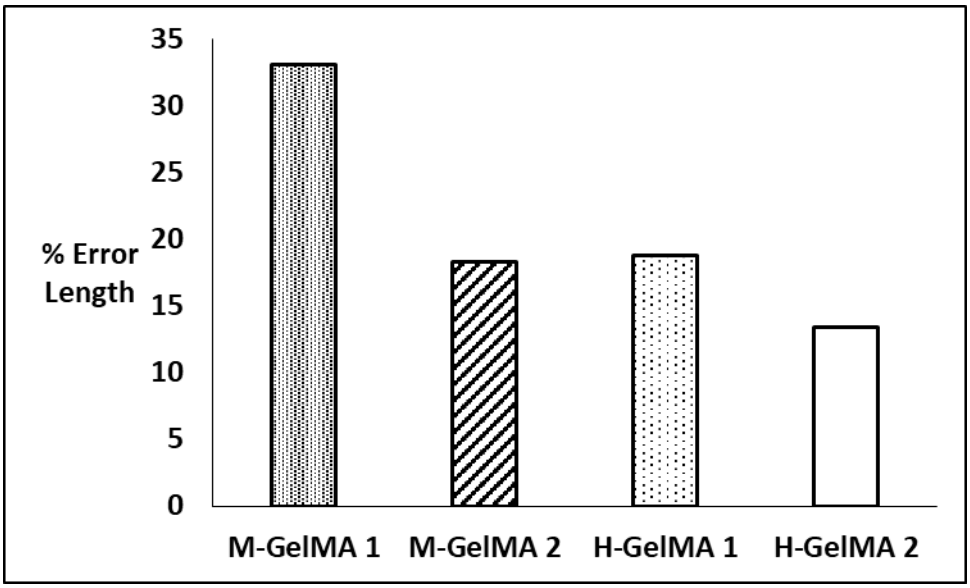

Figure 3-9: A) Pore height measurements and standard deviations for faces of GelMA scaffolds and resins (n = 10). M-GelMA 1 is significantly different than all other resins ($^{*}p < 0.001$). H-GelMA 1 is significantly different than M-GelMA 1 ($^{**}p < 0.001$). Lastly, H-GelMA 2 is significantly different than M-GelMA 1 and M-GelMA 2 ($^{\#}p < 0.005$) in terms of the pore height measurements. B) Percent error bar graph depicting the deviation between GelMA Resins and the theoretical pore height measurements.

Next, the top of scaffold pore width measurements were analyzed (Figure 3-11). The same trends as that observed in Figure 3-10 were observed in Figure 3-11. H-GelMA 2 was significantly larger than both M-GelMA 1 and M-GelMA 2 ($p < 0.005$) in terms of pore width. H-GelMA 1 was only significantly different than M-GelMA 1 ($p < 0.001$), suggesting that at lower concentrations of GelMA and higher concentrations of UV blocker, M-GelMA 2 and H-GelMA 1 behave similarly. The overall trend revealed that M-GelMA 1 does not produce good 3D prints. Figure 3-11B, shows that H-GelMA 2 has the lowest percentage of error in terms of the pore width measurements, making it the overall best printing resin within this category. The % error in pore width for M-GelMA 2, H-GelMA 1, and H-GelMA 2 all fell between 10-20%, meaning these prints were "good" in terms of pore width. M-GelMA 1 was above 20% error and was deemed a "poor" print.

A)

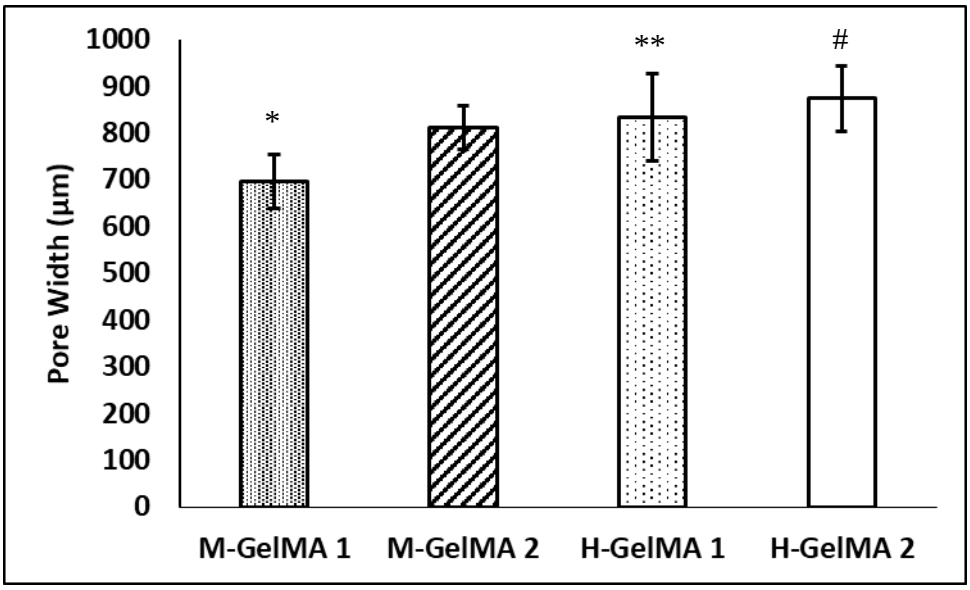

B)

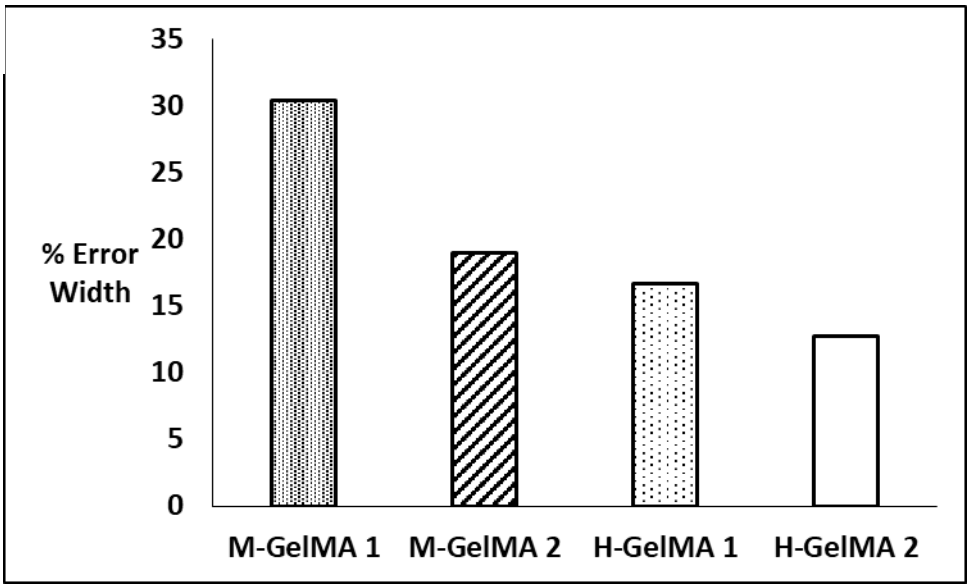

Figure 3-10: A) Pore width measurements and standard deviations for faces of GelMA scaffolds and resins (n = 10). M-GelMA 1 was significantly different than all other resins ($^{*}p < 0.001$). H-GelMA 1 is significantly different than M-GelMA 1 ($^{**}p < 0.001$). Lastly, H-GelMA 2 was significantly different than M-GelMA 1 and M-GelMA 2 ($^{\#}p < 0.005$) in terms of the pore width measurements. B) Percent error bar graph depicting the deviation between GelMA Resins and the theoretical pore width measurements.

3.6.3 Bulk Scaffold Measurements

The bulk scaffold measurements (Figure 3-7A) include the total scaffold height and total scaffold width. Similar to scaffold face pore height measurements, there was significance across formulations for scaffold height measurements (Figure 3-12). Two outstanding observations were that: M-GelMA 1 was significantly smaller in terms of scaffold height than all other resins, H-GelMA 2 was significantly taller than all other formulations, and M-GelMA 2 and H-GelMA 1 were not significantly different. M-GelMA 1 was unable to reach the 4 mm intended height of the scaffold. This could indicate there was an error within the 3D printer itself (i.e. over cure or under cure occurred), or there were material limitations for what can and cannot be printed with this µSL system (i.e. the prints could have been collapsing on themselves). Additionally, the

geometry of the print may play a role in print fidelity. These sources of error can be derived from the working curve (see Section 3.5) as well as the instrumental error (see Section 2.5.2). If the critical exposure and depth of penetration are below or beyond the limitations of the projector used in the instrument, then it is likely to encounter errors where the intended structure cannot be produced. Sources of instrumental error include that the layer height is mediated by the build platform's stepper motor. Calibration during printer setup can cause small deviations where a layer is either over or under exposed. The focal length of the projector is also sensitive to movement, which can cause small deviations in the projection and affect the overall bulk dimensions of the scaffold. Another source of error for M-GelMA 1 could be that since M-GelMA 1 would have less methacrylate groups per volume, M-GelMA 1 could be experiencing less crosslinking. Similar to the trends found in Figure 3-9 through Figure 3-11, H-GelMA 2 has the lowest % error among all other resins. H-GelMA 2 is the most promising resin for producing precise scaffolds with this µSL system while maintaining the highest scaffold fidelity. In terms of scaffold height M-GelMA 2, H-GelMA 1, and H-GelMA 2 all fell within 5-10% error, deeming them "very good" prints. M-GelMA 1 fell within the 10-20% range for scaffold height, deeming it a "good" print in this category.

A)

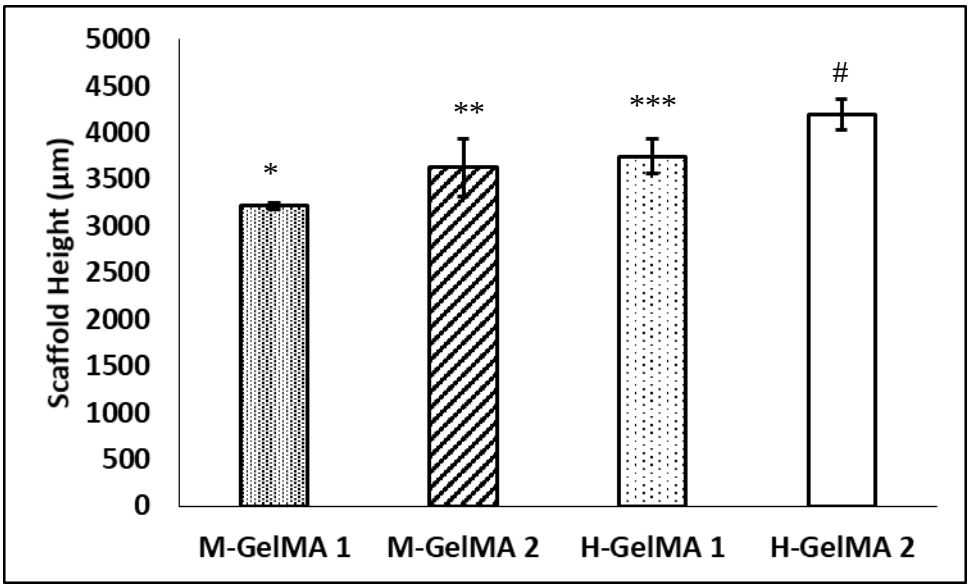

B)

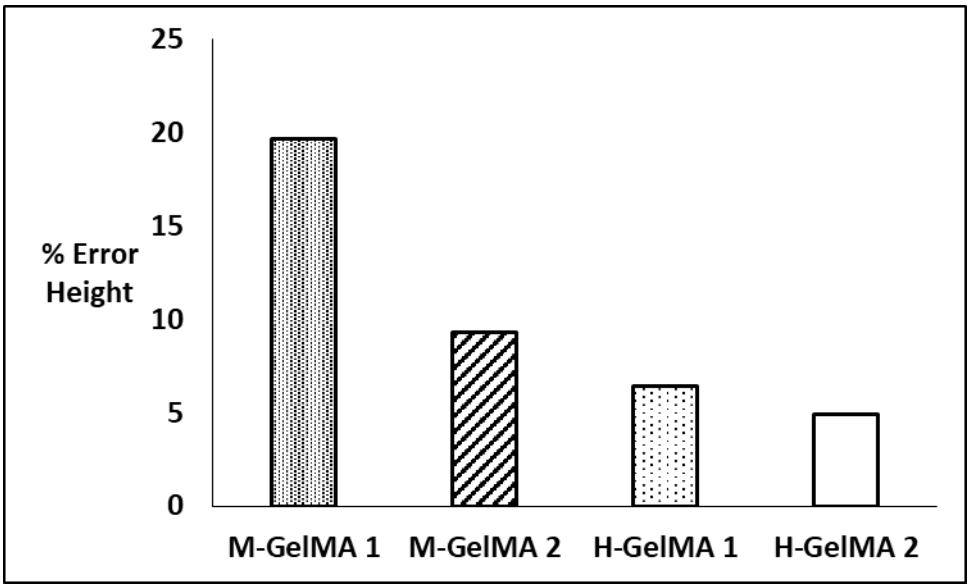

Figure 3-11: A) Scaffold height measurements and standard deviations for bulk GelMA scaffolds (n = 10). M-GelMA 1 is significantly different than all other resins ($^{*}p < 0.05$). M-GelMA 2 is significantly different than M-GelMA 1 and H-GelMA 2 ($^{**}p < 0.05$). H-GelMA 1 is significantly different than M-GelMA 1 and H-GelMA 2 ($^{***}p < 0.05$). Lastly, compared to all other groups H-GelMA 2 is significantly different ($^{\#}p < 0.05$) than all other GelMA resins in terms of the scaffold height measurements. B) Percent error bar graph depicting the deviation between GelMA Resins and the theoretical scaffold height measurements.

Next, the total scaffold width was measured and analyzed in the same way as the scaffold height. Unlike with the scaffold height measurements, H-GelMA 2 scaffold widths were significant larger (Figure 3-13A, $p < 0.05$) compared to other formulations. Once more H-GelMA 2 reported

the lowest % error in terms of the total scaffold width. The same observation regarding the total scaffold height was seen for M-GelMA 1 and M-GelMA 2 in terms of scaffold width. For all formulations, the scaffold width reported was not close to the 4 mm intended width. This could be attributed to the instrumental error described above. In terms of printability, H-GelMA 2 fell within the 10-20% error category, producing a "good" print while the rest of the formulations were greater than 20% error, deeming them "poor" prints.

A)

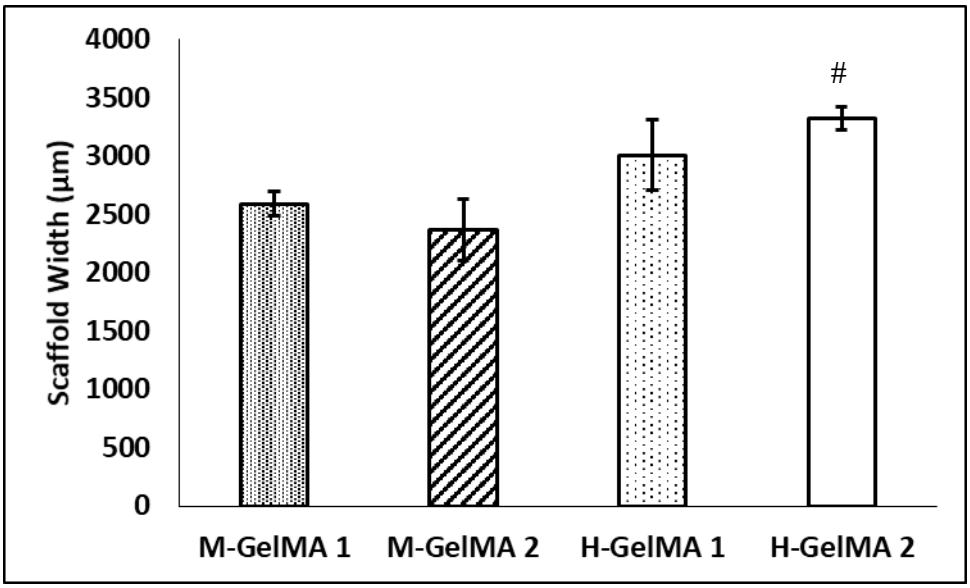

B)

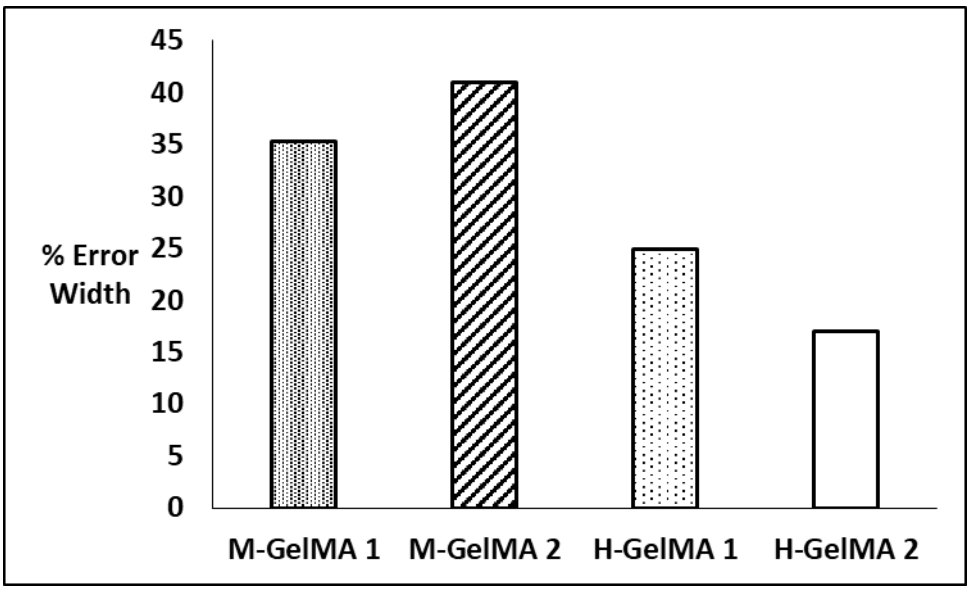

Figure 3-12: A) Scaffold width measurements and standard deviations for bulk GelMA scaffolds (n = 10). Compare to all other resins, H-GelMA 2 is significantly different ($^{\#}p < 0.05$) in terms of the scaffold width measurements. B) Percent error bar graph depicting the deviation between GelMA Resins and the theoretical scaffold width measurements.

3.6.4 Scaffold Layer Measurements

Lastly, the scaffold layer measurements were measured and analyzed. The input parameter in the LabView program was 100 µm. Figure 3-13A depicts the various reported layer heights across scaffolds. Statistical analysis determined all layer height measurements were significantly different than one another ($p < 0.05$). In terms of print fidelity Figure 3-13B surprisingly revealed M-GelMA 1 had the lowest % error in terms of the layer measurement. This is surprising because in almost all other categories of print fidelity, M-GelMA 1 failed to meet the desired printability parameters set. It was also interesting to report that H-GelMA 2, which had the lowest % error in every other category, had the second highest % error in respect to layer height. The additional layer height may be a product of why H-GelMA 2 met the fidelity requirements for bulk scaffold measurements (total scaffold width and total scaffold height). Since H-GelMA 2 has the highest concentration of GelMA and UV blocker, it had the second highest exposure time (Figure 3-7C). A higher exposure time is needed to cure layers because the UV blocker scavenges free radicals needed to induce crosslinking. M-GelMA 1 and H-GelMA 1 had the lowest amount of UV blocker, but Figure 3-13A demonstrates that H-GelMA 1 could not maintain 100 µm layers. The working curve also predicts this observation. (H-GelMA 1 has the highest depth of penetration). In terms of print fidelity, since M-GelMA 1 feel within the 1-5% error range it was deemed a “very good” print. All other resin formulations had greater than 20% error in terms of layer height, deeming them “poor” prints.

A)

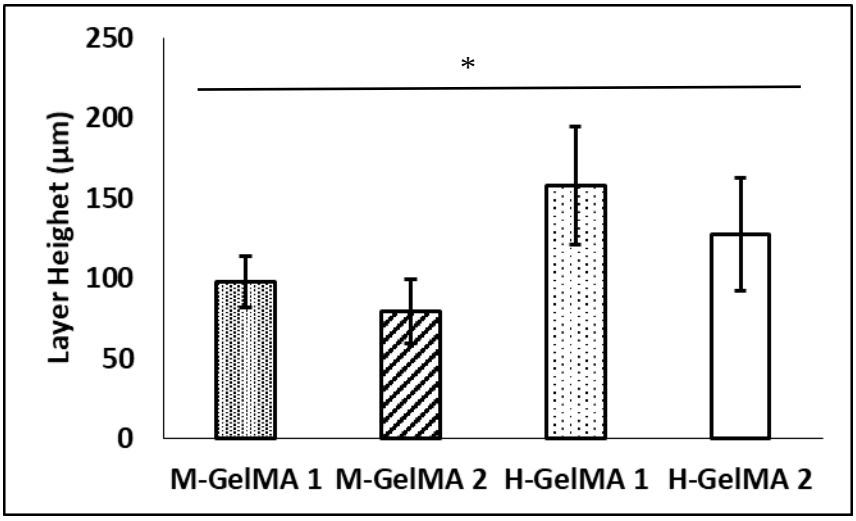

B)

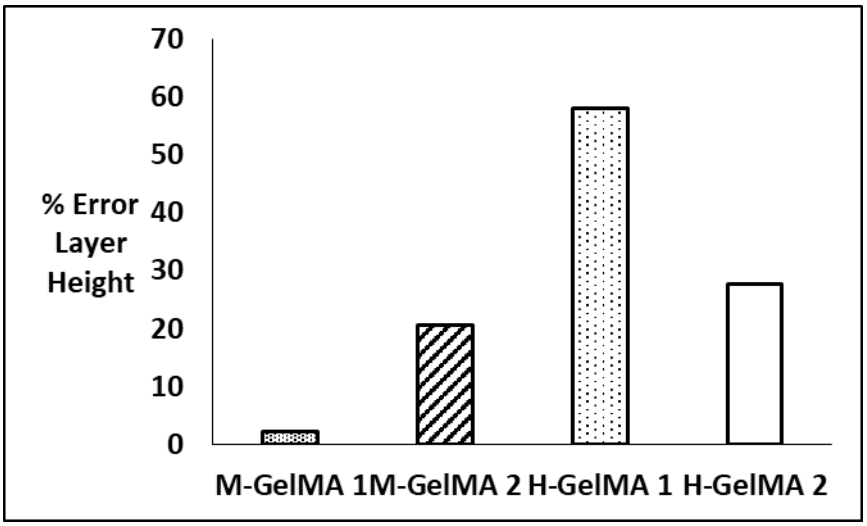

Figure 3-13: A) Scaffold layer measurements and standard deviations for bulk GelMA scaffolds (n = 10). Significance was determined between all resin types regarding the scaffold layer measurements ($^{*}p < 0.05$). B) Percent error bar graph depicting the deviation between GelMA Resins and the theoretical pore height measurements.

Table 3-2 summarizes the analyzed printability of all GelMA formulations. The resin formulation that had the most "good" and "very good" printability rankings was H-GelMA 2. Overall, H-GelMA 2 was the only formulation able to resolve the closest desired porosity in the XY, XZ, and YZ direction. H-GelMA 2 only lacked fidelity in terms of the layer height. Although M-GelMA 1 and H-GelMA 1 were able to resolve porosity at the top of the scaffold, they failed in terms of the XZ and YZ tolerances. M-GelMA 1 resolved the best layer height.

This was due to the fact it had the lowest monomer concentration as well as the lowest UV blocker concentration and likely led to under curing. As described in section 2.5.2, this particular instrument lacks z-directional accuracy, and even Lambert reported errors of 100% in terms of the z-accuracy, so tailoring the proper layer height would require a formulation that likely has higher UV blocker concentration if the monomer concentration is above 30% w/w GelMA. The working curve data predicted that M-GelMA 2 would have performed the best due to the low depth of penetration and critical exposure time. This should have allowed the resin to reach layer heights as low at 35 μm. However, in application, M-GelMA 2 tied for second best formulation with H-GelMA 1, with M-GelMA 1 being the worst. Even at 1 s exposure, M-GelMA 2 could not generate consecutive layers and produce a 3D scaffold.

Table 3-3: Summary of printability for GelMA Resin Formulations.

	M-GelMA 1	**M-GelMA 2**	**H-GelMA 1**	**H-GelMA 2**
Pore Height (face)	Poor	Poor	Poor	Good
Pore Width (face)	Poor	Poor	Poor	Good
Pore Length (top)	Poor	Good	Good	Good
Pore Width (top)	Poor	Good	Good	Good
Scaffold Width	Good	Good	Good	Very Good
Scaffold Height	Poor	Poor	Poor	Good
Layer Height	Very Good	Poor	Poor	Poor

3.7 Cell Culture

GelMA is ubiquitous in its biological applications due to its inherent biocompatibility [16, 33, 35, 38, 42, 52, 53, 55, 56, 59]. Multitudes of researchers have examined cell viability,

biocompatibility, and cell proliferation with various GelMA compositions, all reporting viability above 80% [16, 33, 35, 38, 42, 52, 53, 55, 56, 59]. GelMA concentrations tested in cell culture range from 10 – 20% w/v, with an observed increase in viability with an increase in GelMA concentration [16, 33, 35, 38, 42, 52, 53, 55, 56, 59]. This is because the higher GelMA concentration corresponds to more RGD sequences on the polymeric backbone that the cells recognize for signaling and proliferation. Results from 1 and 3 day cell culture studies are shown below in Figure 3-14. At 1 day, no significant difference in cell density was found between resin formulations or the control. At 3 day, no difference was found between resin formulations. However, the 3 day control was significantly higher ($p < 0.05$) than all resin types. This could indicate at 1 day, the samples behaved similar to the control, but at 3 days there was a reduced cell density compared to the control. Potentially, cell growth or attachment could be delayed on GelMA films with LAP and sulisobenzone. Further analysis of a 7 day or 14 day study may prove the cell density would recover to be similar that of the control. No significant difference was found between UV blocker concentration and cell density within these GelMA resins. Between 1 and 3 day studies there was significance increase in cell density across all resin types and the controls. This was a positive result because it validates the cell density did increase over the allotted time period, meaning the GelMA formulations developed are biocompatible and do support cell growth/adhesion. Cell staining was also performed to observe qualitative responses to GelMA films *in vitro* (Figure 3-15). By 3 day, the cells became more spindle-like shape and were more clustered compared to 1 day, this visually confirmed the cell density has increased.

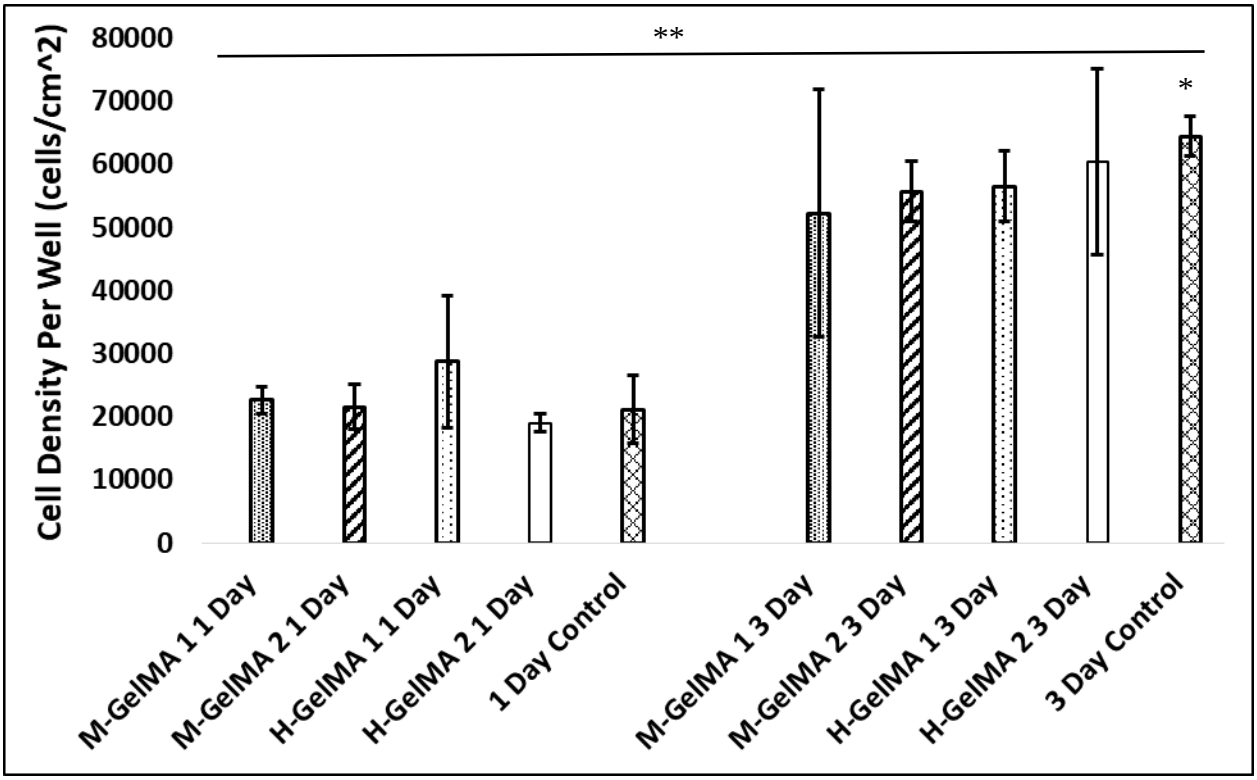

Figure 3-14: Cell culture study results for 1 and 3 day studies. Experiments were run in triplicate (n = 3). At 1 day, no significant difference was observed between resins as well as between the resins and control ($p > 0.05$). For 3 day, no significance was observed between resins, but there was significance between each resin and the control ($^{*}p < 0.05$). Further statistical analysis between 1 and 3 days revealed that for each resin type there was a significance between 1 and 3 days of cell culture (i.e. M-GelMA 1 at 1 day was significantly different than M-GelMA 1 at 3 day) ($^{**}p < 0.05$).

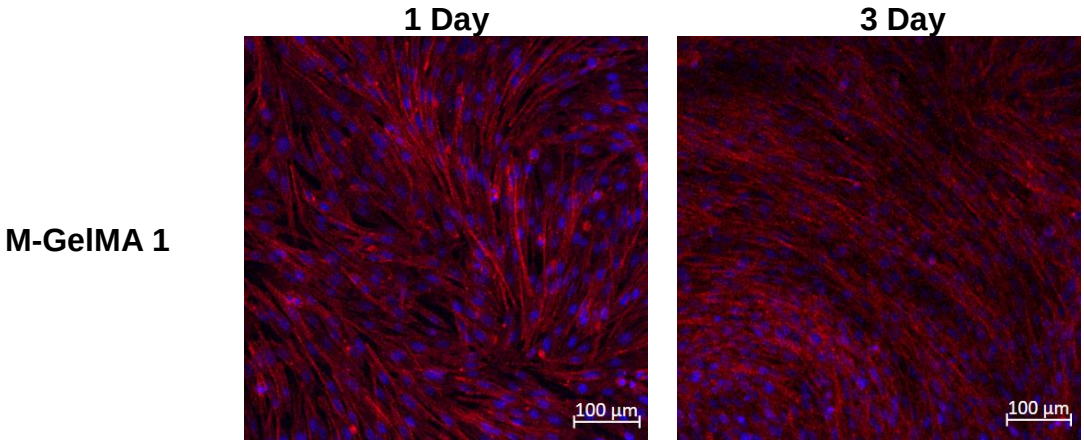

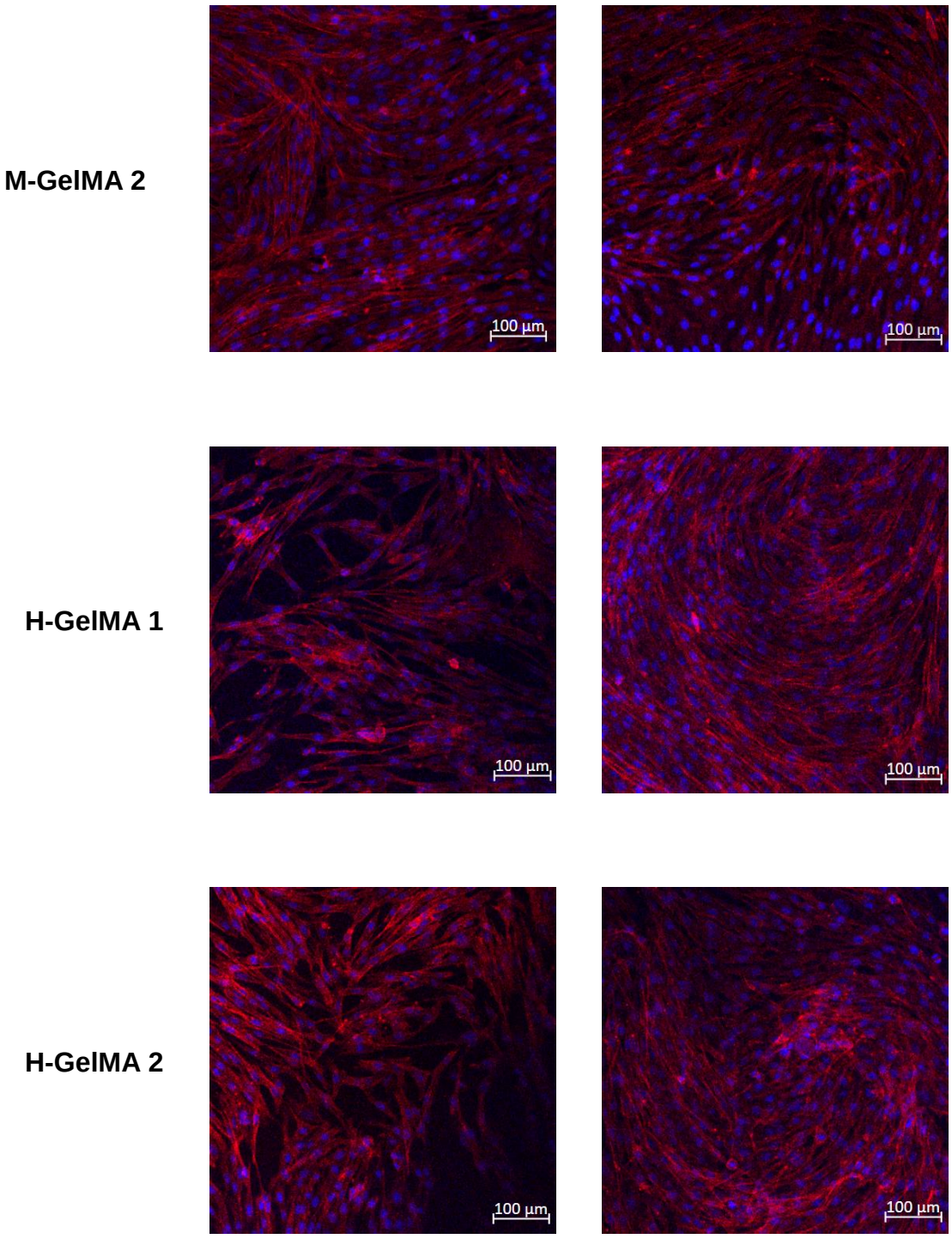

Figure 3-15: Representative light microscopy images of GelMA films seeded with 3T3s and stained for nuclei (DAPI, blue) and actin (Texas Red, red).
Experiments were run in triplicate (n = 3)

Chapter 4: Conclusions and Future Directions

4.1 Conclusions

Developing a novel biomaterial resin for use in µSLA comes with its challenges. This work successfully developed, characterized, and 3D printed a novel gelatin methacrylate resin for use in µSL. The significant contribution to the field was the fidelity and resolution achieved in the z-direction of each print. In the past, scientists have only proven to alter the surface of GelMA resins creating 2D microstructures, 2D micropatterns, or "3D" prints less than 2 mm in height and lack complexity in the z-direction. This work has demonstrated that the limits of GelMA can be pushed to produce taller structures that utilize the high resolution of µSL printing. In the work described, six novel GelMA resins were formulated and produced for use in µSL. Two resins at lower GelMA concentrations were deemed incompatible due to miscibility issues, and this was validated with photo-rheology and photo-DSC, which proved the reactivity and cure times of those formulations was not ideal for µSL. Of the remaining four formulations, all were characterized prior to 3D printing to gain insight into what parameters to expect for 3D printing.

Once scaffolds were printed, an approach was developed to quantify the fidelity achieved with GelMA resins by measuring features including: pore height, pore width, pore length, scaffold height, scaffold width, and layer height via optical microscopy. The best resin was determined based off of the % error from the .STL file from which the 3D print was produced. One resin was identified as a stepping stone for future work. The H-GelMA 2 resin proved to retain its fidelity and had the lowest error percentage compared to the original .STL file from which it was printed. Not only were prints with H-GelMA 2 resin visually more successful than the other resins, but a

method was developed to quantify the printability of the system. The printability was defined using a semi-quantitative method. This method utilized optical microscopy to measure feature sizes, and a ranking system based off of the instrumental tolerances of the µSLA printer to categorize prints as either “very good” “good” or “poor.”

The two specific aims of this work were to:

1. Develop a novel GelMA resin that can print a 3D scaffold with a height greater than 2 mm. This resin should also improve on the overall cure time of the scaffold produced.
2. Display the complexity of µSL with this novel GelMA resin by being able to produce a scaffold with porosity and pore sizes of 1000 µm, and a layer thickness less than 200 µm.

Aim 1 was fully addressed. In all formulations a scaffold height greater than 2 mm was produced. And the longest recorded print time for a scaffold was less than 5 minutes. In aim 2, the goal was to produce 1000 µm pores based off of the print file. As shown in the work, the highest pore size (width and height) achieved was 800 µm on scaffold faces. However, a layer thickness less than 200 µm was achieved for all resin formulations.

4.2 Significance

This work is significant because for the first time reported in µSLA, a structure was produced with GelMA that had a z-height greater than 2 mm and layer thickness close to 100 µm, which has not been demonstrated before. Additionally, this resin was deemed biocompatible after cell culture studies verified an increase in cell density from 1 to 3 days. This opens the door for a

world of applications in tissue engineering, regenerative medicine, drug screening, pre-surgical planning, and 3D bioprinting with µSL and GelMA.

Another significant contribution of this work to the additive manufacturing and 3D printing community is the comprehensive characterization approach with semi-quantitative print fidelity rankings. There is a lack of standardized quantification that exists to differentiate different systems and material developed for 3D printing. This work demonstrates numerous characterization techniques: photo-rheology, photo-DSC, working curve, and optical microscopy analysis to characterize rheological properties, reaction kinetics, printability parameters, and print fidelity respectively. Most literature does not utilize fidelity measurements to validate printability, which begs the question of how can we, as a scientific community, prove our 3D print system is successful. Although a material may produce a scaffold or geometry, how do we judge or define whether or not that design or printed part is successful? Additionally, the statistical analysis performed on this work validates the characterization methods used were indeed significant. The reported results and statistical analysis confirmed trends relating to material properties seen in previous literature, as well as trends in the overall printability of resins. This work systematically defines GelMA formulations that were or were not compatible for µSL printing. The L-GelMA resin formulations, containing 10% GelMA, failed to reach the printing stage as their rheological properties could not be reliably measured, and their specific heat and cure times were too low to warrant processing via µSL. This was attributed to a lack of solubility between the UV blocker and GelMA, where L-GelMA 1 resins were still turbid, but clearer than L-GelMA 2 resins.

The H-GelMA 2 resin was the most successful in terms of printability. From photo-rheology, the H-GelMA 2 resin exhibited a storage modulus around 400 kPA and a gel point around 3 s. From photo-DSC, the H-GelMA 2 resin exhibited a specific heat around 3 J/g and total cure time around 40 s. The H-GelMA 2 formulation swelled approximately 240% and had a depth of penetration of 80 µm and critical exposure of 1400 ms. H-GelMA 2 reported the best print fidelity, ranking highest in 5 categories out of 6. Additionally the biocompatibility of the H-GelMA 2 resin was proved successful. After 3 days, the cell density on H-GelMA films increased 300%. This is a great starting point for producing larger constructs of GelMA via µSL, however, there is plenty of room for future work and improvements.

4.3 Future Directions

Future work regarding this project can lead in multiple directions: 1. focusing on the raw materials/synthesis of GelMA; 2. focusing on the printable shape/3D construct; and 3. altering the concentrations of components within the resin further. These future directions are primarily focused on the µSL application of GelMA since the work described contributes to a novel resin formulation and print fidelity analysis not seen in prior literature. Applications for GelMA range from wound healing constructs, to neural repair and regeneration, and even tendon and ligament formation. Ideally, the same approach developed in this work could be used as a benchmark for various different resin formulations tested in µSL, not just GelMA and hydrogel printing. Especially in the tissue engineering community there is a push to understand the cellular microenvironment and cell interactions based off of mechanical cues and geometry. The µSL

application of GelMA would allow researchers to create larger constructs that mimic the geometry and material properties found *in vivo*.

The synthesis of GelMA would be an interesting point for future analysis because varying the DS could have impacts on the cure time and reactivity of the resin. As discussed, in this work an average of 54% DS was achieved. Aiming for 90-99% DS would alter the reactivity and exposure times needed for printing. Additionally, at 99% DS, a 10% w/v GelMA resin may print similar to 20% or 30% respectively. Solubility tests would be essential to first see if a higher DS would prevent turbid solutions from forming. Printing at a lower concentration of GelMA would allow researchers to produce GelMA scaffolds with lower storage moduli and greater swelling, which for different applications in organ printing or cell types would be useful.

The 3D print file is another point of future work. In this work, a simple window structure was analyzed as a benchmark for improving on the z-height and complexity of GelMA prints in literature. As a proof of concept, the H-GelMA 2 resin was successful, but how would this vary based on the layer height and printed shape. What if the shape were conical? Or had circular pores? Would over curing be more or less noticeable? Some limitations on the printed shape depend solely on the machine on which they are printed. For example, the resolution of the printer used in this work should theoretically be 10 µm, but when Lambert tested the system they commented the pixel size has an error of 2 µm, and the smallest feature they were able to cure was 20 µm, not 10 µm. Material properties are of great concern, and with GelMA, over curing was a common issue. The refraction of light within the construct during printing can cause issues as well. Potentially with this chosen geometry may exhibit more or less over cure than a different

geometry. Also, this is an open system, meaning oxygen on the surface of the resin during printing can act as an inhibitor. This could result in longer exposure times on the resin surface, which may ultimately lead to over cure. More optical image analysis would be required to test different geometries with the same resin formulation to observe this phenomenon. Additionally, the impact of swelling on the 3D printed part could be further explored. If the swelling is truly making an impact on the print fidelity, further analysis would be needed to verify this.

The resin formulation is always an area for discovery. Especially with regards to this work, increasing the UV blocker concentration from 1.0% to perhaps even 2.0% may drastically improve the fidelity of printed constructs. Higher UV blocker concentration may increase exposure time, but reduce layer height and improve on the overall fidelity of the structure. Increasing the UV blocker concentration would cause concern for the biocompatibility of the formulation. More UV blocker or photoinitiator may introduce more cytotoxicity into the resin formulation and reduce cell viability. There may also be a solubility concern at higher UV blocker concentrations. Developing a phase diagram to observe the upper or lower limit of solubility of formulation components would be incredibly useful. Just as the L-GelMA resins were turbid and had immiscible components, this same effect may be observed at higher concentrations of UV blocker relative to the GelMA concentration.

In closing, this work pushes the current work surrounding 3D printing and GelMA. Prior work with µSL printing GelMA produced 2D or “2.5D” scaffolds, or a 3D scaffold that would take nearly 6 hours to produce. This work also comments on the lack of characterization in terms of print fidelity within the 3D printing community. Machine tolerances and error percentages need

to be considered. Simply being able to produce a pattern or scaffold with a scale bar should not be the only characterization of fidelity. The H-GelMA 2 resin and printability analysis method are a great start for future µSL printing with gelatin methacrylate and this system to further push the boundaries of GelMA printing with µSL.

Appendix A:

Appendix A lists the various resin formulations tested as a part of preliminary resin development. Each section is commented on respectively.

Other Characteristics	-Thin films swell a lot -No print picture available but it did print a porous structure -Thin films seemed brittle -Solubility issues with DMPA and AMPS/H2O -Additionally went down in H2O concentration to 20%	-Films seemed to crack a lot -Had trouble with the sterilization
Biocompatibility	Tested results indicated poor viability)	Tested (cells died after 3 days)
3D Print?	Yes	N/A
Layer Thickness (Printer)	~250 um	N/A
Cure Time (Printer)	10 sec	N/A
Cure Time (UV Lamp)	30 sec	1 min
Resin Composition (w/w %)	20% GelMA 50% Amps 10% Hema 25% H2O 1% DMPA 1% Sulisobenzone	20% GelMA 50% Amps 10% Hema 25% H2O 1% DMPA 0.05% Avobenzone
Date	9/11/2017	9/27/2017

-Long exposure time per film creation -Printing required alternative light source	-This resin formulation did not work	-Was able to print window structure -Solution mainly made of PEGDA and AMPS -In cell culture tried removing sulisobenzone and even increasing GelMA -Miscibility issues and shielding occurring during curing?
Tested (cells grew)	N/A	Tested (no adhesion cell viability not apparent)
No	No	Yes
N/A	N/A	~140 um
N/A	N/A	1 sec
5 min	N/A	Less than 20 sec
20% GelMA 50% Amps 10% Hema 20% H2O 1% Irgacure 2959 0.05% Sulisobenzone	22.5% GelMA 55% Amps 22.5% H2O 2% Irgacure 819 (BAPO) 0.5% Sulisobenzone	10% GelMA 30% Amps 30% PEGDA 30% H2O 1% DMPA 0.5% Sulisobenzone
11/3/2017	11/6/2017	11/14/2017

-Evaporation of ethanol contributed to a film forming on the resin surface -Did print a solid block with 0.3% sulisobenzone, but the resin just will not print due to ethanol evaporation	-Long print/cure time -Films swell a lot	-First print of building structure was semi-successful -Print parameters can be adjusted to reduce layer thickness potentially, but may cause over cure
Tested (cells grew but did not appear as confluent as controls, but good)	Tested (cells grew, looked confluent, but MTS conflicts with DMSO?)	N/A
No	No (solid	Yes
N/A	N/A	~200 um/greater than this
N/A	50 sec	3 sec
10 sec	1.5 min	5 sec
30% GelMA 55% EtOH (70%) 15% H2O 1% DMPA	30% GelMA 70% DMSO 1% DMPA 0.3% Sulisobenzone	20% GelMA 80% H2O 0.5% LAP 0.5% Sulisobenzone
12/1/2017	1/25/2018	1/26/2018

-Window part structure kept coming out like a "pagoda" -Over curing/under curing occurring due to lack of photoinitiator and higher conc. of UV blocker	-Was able to produce the best printed structure far -Varying exposure time on the printer affected layer thickness and porosity -Struggle with some over curing -Printed multiple geometries	N/A	Yes	~150 um/greater than this	10 sec	15 sec	20% GelMA 80% H2O 0.1% LAP 0.5% Sulisobenzone	2/6/2018
N/A	N/A	Yes	200 um 100 um	3.75 sec 1.8 sec	N/A	20% GelMA 80% H2O 0.5% LAP 1% Sulisobenzone	2/8/2018	

In Appendix A, numerous resin formulations were developed and tested for their biocompatibility and printing parameters with the uSL printer. The GelMA, water, LAP, and sulisobenzone resins had the most promising results and this is how it was determined to continue moving forward with this particular resin type (See date: 2/8/2018).

References:

[1] R. D. Gibson I., Stucker B., *Additive Manufacturing Technologies*. New York, NY: Springer, 2015.

[2] I. Donderwinkel, van Hest, J. C. M. and Cameron, N. R., "Bio-inks for 3D bioprinting: recent advances and future prospects," *Polymer Chemistry,* vol. 8, no. 31, pp. 4451-4471, 2017.

[3] N. C. Philip Lambert, Alison Schultz, Shelley Cooke, Timothy Long, Abby Whittington, Christopher Williams and "Mask Projection Microstereolithography of Novel Biocompatible Polymers " presented at the 16th Annual Conference of the North Carolina Tissue Engineering and Regenerative Medicine Society, Durham, NC, 2014.

[4] A. A. Sean V Murphy, "3D bioprinting of tissues and organs," *Nature Biotechnology,* vol. 32, no. 8, pp. 773-785, 2014.

[5] T. Jungst, Smolan, W., Schacht, K., Scheibel, T. and Groll, J., "Strategies and Molecular Design Criteria for 3D Printable Hydrogels," *Chemical Reviews,* vol. 116, no. 3, pp. 1496-1539, 2015 2015.

[6] W. Y. Y. J.M Lee, "Design and Printing Strategies in 3D Bioprinting of Cell-Hydrogels: A Review," *Advanced Healthcare Materials,* vol. 5, no. 22, pp. 2856-2865, 2016.

[7] J. R. Jones, "Observing cell response to biomaterials," *Materials Today,* vol. 9, no. 12, pp. 34-43, 2006.

[8] Y. Seol, Kang, H., Lee, S. J., Atala, A. and Yoo, J. J., "Bioprinting technology and its applications," *European Journal of Cardio-Thoracic Surgery,* vol. 46, no. 3, pp. 342-348, 2014.

[9] P. Lambert, "Design and Fabrication of a Mask Projection Microstereolithography System for the Characterization and Processing of Novel Photopolymer Resins " M.S, Mechanical Engineering, Virginia Tech, 2014.

[10] N. I. o. Health. (8). *Tissue Engineering and Regenerative Medicine*. Available: https://www.nibib.nih.gov/science-education/science-topics/tissue-engineering-and-regenerative-medicine

[11] B. M. W. H. N. Chia, "Recent advances in 3D printing of biomaterials," *Journal of Biological Engineering,* vol. 9, no. 1, 2015.

[12] Q. L. a. C. Choong, "Three-Dimensional Scaffolds for Tissue Engineering Applications: Role of Porosity and Pore Size," *Tissue Engineering Part B: Reviews,* vol. 19, no. 6, pp. 485-502, 2013.

[13] F. M. J. Jansen, D. Grijpma and J. Feijen, "Fumaric Acid Monoethyl Ester-Functionalized Poly(d,l-lactide)/N-vinyl-2-pyrrolidone Resins for the Preparation of Tissue Engineering Scaffolds by Stereolithography," *Biomacromolecules,* vol. 10, no. 2, pp. 214-220, 2009.

[14] R. W. J. Choi, S. Lee, K. Choi, C. Ha and I. Chung, "Fabrication of 3D biocompatible/biodegradable micro-scaffolds using dynamic mask projection microstereolithography," *Journal of Materials Processing Technology,* vol. 209, no. 15-16, pp. 5494-5503, 2009.

[15] S. Skoog, Goering, P. and Narayan, R., "Stereolithography in tissue engineering," *Journal of Materials Science Materials in Medicine,* vol. 25, no. 3, pp. 845-856., 2013.

[16] K. Kim, Dean, D., Wallace, J., Breithaupt, R., Mikos, A. and Fisher, J., "The influence of stereolithographic scaffold architecture and composition on osteogenic signal expression

with rat bone marrow stromal cells. Biomaterials," *Biomaterials,* vol. 32, no. 15, pp. 3750-3763, 2011.

[17] S. Lee, Kang, H., Park, J., Rhie, J., Hahn, S. and Cho, D, "Application of microstereolithography in the development of three-dimensional cartilage regeneration scaffolds," *Biomedical Microdevices,* vol. 10, no. 2, 2007.

[18] M. Schuster, Turecek, C., Kaiser, B., Stampfl, J., Liska, R. and Varga, F. (2007). Evaluation of Biocompatible Photopolymers I: Photoreactivity and Mechanical Properties of Reactive Diluents. Journal of Macromolecular Science, Part A, 44(5), pp.547-557., "Evaluation of Biocompatible Photopolymers I: Photoreactivity and Mechanical Properties of Reactive Diluents," *Journal of Macromolecular Science, Part A,* vol. 44, no. 5, pp. 547-557, 2007.

[19] F. C. Andrew A. Gill, Haycock, J., "3D Structuring of Biocompatible and Biodegradable Polymers Via Stereolithography," in *3D cell culture*, vol. 3rd ed, J. Haycock, Ed. Totowa, N.J.: Humana Press, 2011, pp. 309-321.

[20] M. a. M. Mizutani, T. (2002). Liquid photocurable biodegradable copolymers: In vivo degradation of photocured poly(ε-caprolactone-co-trimethylene carbonate). Journal of Biomedical Materials Research, 61(1), pp.53-60., "Liquid photocurable biodegradable copolymers: In vivo degradation of photocured poly(ε-caprolactone-co-trimethylene carbonate)," *Journal of Biomedical Materials Research,* vol. 61, no. 1, pp. 53-60, 2002.

[21] K. Arcaute, Mann, B. and Wicker, R. (2010). Stereolithography of spatially controlled multi-material bioactive poly(ethylene glycol) scaffolds. Acta Biomaterialia, 6(3), pp.1047-1054., "Stereolithography of spatially controlled multi-material bioactive poly(ethylene glycol) scaffolds," *Acta Biomaterialia,* vol. 6, no. 3, pp. 1047-1054, 2010.

[22] H. Sung, Meredith, C., Johnson, C. and Galis, Z. , "The effect of scaffold degradation rate on three-dimensional cell growth and angiogenesis," *Biomaterials,* vol. 25, no. 26, pp. 5735-5742, 2004.

[23] W. C. J. Dunn, V. Cristini, J. Kim, J. Lowengrub, S. Singh and B. Wu, "Analysis of Cell Growth in Three-Dimensional Scaffolds," *Tissue Engineering,* vol. 12, no. 4, pp. 705-716, 2006.

[24] H. Shirahama, Lee, B., Tan, L. and Cho, N., "Precise Tuning of Facile One-Pot Gelatin Methacryloyl (GelMA) Synthesis," *Scientific Reports,* vol. 6, no. 1, 2016.

[25] K. Yue, Trujillo-de Santiago, G., Alvarez, M., Tamayol, A., Annabi, N. and Khademhosseini, A. , "Synthesis, properties, and biomedical applications of gelatin methacryloyl (GelMA) hydrogels," *Biomaterials,* vol. 73, pp. 254-271, 2015.

[26] M. A. Carletti E., Migliaresi C, "Scaffolds for Tissue Engineering and 3D Cell Culture," in *3D Cell Culture. Methods in Molecular Biology (Methods and Protocols),* vol. 695, H. J., Ed.: Humana Press, 2011.

[27] P. Zorlutuna, Jeong, J., Kong, H. and Bashir, R., "Tissue Engineering: Stereolithography-Based Hydrogel Microenvironments to Examine Cellular Interactions," *Advanced Functional Materials,* vol. 21, no. 19, pp. 3597-3597, 2011.

[28] R. Mondschein, Kanitkar, A., Williams, C., Verbridge, S. and Long, T. , "Polymer structure-property requirements for stereolithographic 3D printing of soft tissue engineering scaffolds," *Biomaterials,* vol. 140, pp. 170-188, 2017.

[29] V. Morris, Nimbalkar, S., Younesi, M., McClellan, P. and Akkus, O. , "Mechanical Properties, Cytocompatibility and Manufacturability of Chitosan:PEGDA Hybrid-Gel

Scaffolds by Stereolithography," *Annals of Biomedical Engineering*, vol. 45, no. 1, pp. 286-296, 2016.
[30] S. Suri, Han, L., Zhang, W., Singh, A., Chen, S. and Schmidt, C. , "Solid freeform fabrication of designer scaffolds of hyaluronic acid for nerve tissue engineering," *Biomedical Microdevices*, vol. 13, no. 6, pp. 983-993, 2011.
[31] H. K. B. Harley, M. Zaman, I. Yannas, D. Lauffenburger and L. Gibson, , "Microarchitecture of Three-Dimensional Scaffolds Influences Cell Migration Behavior via Junction Interactions," *Biophysics Journal*, vol. 95, no. 8, pp. 4013-4024, 2008.
[32] S. F. Charles Molnar and Jane Gair, Rebecca Roush, James Wise, Yael Avissar, Jung Choi, Jean DeSaix, Vladimir Jurukovski, Robert Wise, Connie Rye, *Concepts of Biology-1st Canadian Edition*. B. C. C.: B.C. Open Textbook Project, 2013.
[33] D. Loessner, Meinert, C., Kaemmerer, E., Martine, L., Yue, K., Levett, P., Klein, T., Melchels, F., Khademhosseini, A. and Hutmacher, D. , "Functionalization, preparation and use of cell-laden gelatin methacryloyl–based hydrogels as modular tissue culture platforms," *Nature Protocols*, vol. 11, no. 4, pp. 727-746, 2016.
[34] B. Lee, Lum, N., Seow, L., Lim, P. and Tan, L. , "Synthesis and Characterization of Types A and B Gelatin Methacryloyl for Bioink Applications. Materials," *Materials*, vol. 9, no. 10, p. 797, 2016.
[35] J. Nichol, Koshy, S., Bae, H., Hwang, C., Yamanlar, S. and Khademhosseini, A, " Cell-laden microengineered gelatin methacrylate hydrogels," *Biomaterials*, vol. 31, no. 21, pp. 5536-5544, 2010.
[36] A. Van Den Bulcke, Bogdanov, B., De Rooze, N., Schacht, E., Cornelissen, M. and Berghmans, H.. "Structural and Rheological Properties of Methacrylamide Modified Gelatin Hydrogels," *Biomacromolecules*, vol. 1, no. 1, pp. 31-38, 2000.
[37] T. Lai, Yu, J. and Tsai, W., "Gelatin methacrylate/carboxybetaine methacrylate hydrogels with tunable crosslinking for controlled drug release," *Journal of Materials Chemistry B*, vol. 4, no. 13, pp. 2304-2313, 2016.
[38] H. Lin, Zhang, D., Alexander, P., Yang, G., Tan, J., Cheng, A. and Tuan, R. , "Application of visible light-based projection stereolithography for live cell-scaffold fabrication with designed architecture," *Biomaterials*, vol. 34, no. 2, pp. 331-339, 2013.
[39] L. Xu, Sheybani, N., Yeudall, W. and Yang, H. , "The effect of photoinitiators on intracellular AKT signaling pathway in tissue engineering application," *Biomaterials Science*, vol. 3, no. 2, pp. 250-255, 2015.
[40] S. Wüst, Müller, R. and Hofmann, S. , "Controlled Positioning of Cells in Biomaterials—Approaches Towards 3D Tissue Printing," *Journal of Functional Biomaterials*, vol. 2, no. 4, pp. 119-154, 2011.
[41] D. Kolesky, Truby, R., Gladman, A., Busbee, T., Homan, K. and Lewis, J. , "3D Bioprinting of Vascularized, Heterogeneous Cell-Laden Tissue Constructs," *Advanced Materials*, vol. 26, no. 19, pp. 3124-3130, 2014.
[42] L. Bertassoni, Cardoso, J., Manoharan, V., Cristino, A., Bhise, N., Araujo, W., Zorlutuna, P., Vrana, N., Ghaemmaghami, A., Dokmeci, M. and Khademhosseini, A. , "Direct-write bioprinting of cell-laden methacrylated gelatin hydrogels," *Biofabrication* vol. 6, no. 2, p. 24105, 2014.
[43] B. Fairbanks, Schwartz, M., Bowman, C. and Anseth, K., "Photoinitiated polymerization of PEG-diacrylate with lithium phenyl-2,4,6-trimethylbenzoylphosphinate:

polymerization rate and cytocompatibility," *Biomaterials,* vol. 30, no. 35, pp. 6702-6707, 2009.

[44] A. Ovsianikov, Deiwick, A., Van Vlierberghe, S., Dubruel, P., Möller, L., Dräger, G. and Chichkov, B. , "Laser Fabrication of Three-Dimensional CAD Scaffolds from Photosensitive Gelatin for Applications in Tissue Engineering," *Biomacromolecules,* vol. 12, no. 4, pp. 851-858, 2011.

[45] P. Kim, Yuan, A., Nam, K., Jiao, A. and Kim, D., "Fabrication of poly(ethylene glycol): gelatin methacrylate composite nanostructures with tunable stiffness and degradation for vascular tissue engineering," *Biofabrication,* vol. 6, no. 2, p. 24112, 2014.

[46] A. Skardal, Zhang, J., McCoard, L., Xu, X., Oottamasathien, S. and Prestwich, G. , "Photocrosslinkable Hyaluronan-Gelatin Hydrogels for Two-Step Bioprinting," *Tissue Engineering Part A,* vol. 16, no. 8, pp. 2675-2685, 2010.

[47] M. V. Nicholas A. Chartrain, Dung T. Han, Justin M. Sirrine, Allison Pekkanen, Timothy E. Long, Abby R. Whittington, Christopher B. Williams, "Microstereolithography of Tissue Scaffolds Using a Biodegradable Photocurable Polyester," presented at the Solid Freeform Fabrication 2016: Proceedings of the 26th Annual International Solid Freeform Fabrication Symposium – An Additive Manufacturing Conference Texas, 2016.

[48] M. Chan-Park, Zhu, A., Shen, J. and Fan, A. , "Novel Photopolymerizable Biodegradable Triblock Polymers for Tissue Engineering Scaffolds: Synthesis and Characterization," *Macromolecular Bioscience,* vol. 4, no. 7, pp. 665-673, 2004.

[49] GMIA, Gelatin Handbook, GMIA, ed., 2012. [Online]. Available: http://www.gelatin-gmia.com/images/GMIA_Gelatin_Manual_2012.pdf. Accessed on 2018.

[50] Z. Wang, "Development of a Visibile Light Stereolithography-Based Bioprinting System for Tissue Engineering.," M.S, Mechanical Engineering, The University of British Columbia 2016.

[51] E. McColl, "Using stereolithography to 3D print GelMA hydrogels," M.S, Health and Biomedical Innovation, Queensland University of Technology, 2017.

[52] N. S. P. Occhetta, F. Piraino, A. Redaelli, M. Moretti and M. Rasponi, "Fabrication of 3D cell-laden hydrogel microstructures through photo-mold patterning," *Biofabrication,* vol. 5, no. 3, p. 35002, 2013.

[53] R. V. P. Occhetta, L. Russo, L. Cipolla, M. Moretti and M. Rasponi, "VA-086 methacrylate gelatine photopolymerizable hydrogels: A parametric study for highly biocompatible 3D cell embedding," *Journal of Biomedical Materials Research Part A,* vol. 103, no. 6, pp. 2109-2117, 2014.

[54] J. M. N. Palaganas, A. de Leon, J. Palaganas, K. Pangilinan, Y. Lee and R. Advincula, "3D Printing of Photocurable Cellulose Nanocrystal Composite for Fabrication of Complex Architectures via Stereolithography," *ACS Applied Materials & Interfaces,* vol. 9, no. 39, pp. 34314-34324, 2017.

[55] G. T. N. Monteiro, A. Athirasala, A. Tahayeri, C. França, J. Ferracane and L. Bertassoni, "Photopolymerization of cell-laden gelatin methacryloyl hydrogels using a dental curing light for regenerative dentistry," *Dental Materials,* 2017.

[56] E. G. T. Billiet, T. De Schryver, M. Cornelissen and P. Dubruel, "The 3D printing of gelatin methacrylamide cell-laden tissue-engineered constructs with high cell viability," *Biomaterials,* vol. 35, no. 1, pp. 49-62, 2014.

[57] V. M. B. Golaz, Y. Leterrier, J.-A.E. Månson, "UV intensity, temperature and dark-curing effects in cationicphoto-polymerization of a cycloaliphatic epoxy resin," *Polymer Chemistry*, no. 53, pp. 2038-2048, 2012.
[58] P. Corporation. (2012, March 29 2019). *CellTiter 96® AQueousOne Solution Cell Proliferation Assay*. Available: www.promega.com
[59] X. Q. A. Zhang, P. Soman, K. Hribar, J. Lee, S. Chen and S. He, "Rapid Fabrication of Complex 3D Extracellular Microenvironments by Dynamic Optical Projection Stereolithography," *Advanced Materials*, vol. 24, no. 31, pp. 4266-4270, 2012.